THESIS

THE ROLE OF MOISTURE-CONVECTION FEEDBACKS IN SIMULATING THE INTRASEASONAL OSCILLATION

Submitted by

Walter Hannah

Department of Atmospheric Science

In partial fulfillment of the requirements

For the Degree of Master of Science

Colorado State University

Fort Collins, Colorado

Fall 2009

COLORADO STATE UNIVERSITY

November 9, 2009

WE HEREBY RECOMMEND THAT THE THESIS PREPARED UNDER OUR SUPERVISION BY WALTER HANNAH ENTITLED THE ROLE OF MOISTURE-CONVECTION FEEDBACKS IN SIMULATING THE INTRASEASONAL OSCILLATION BE ACCEPTED AS FULFILLING IN PART REQUIREMENTS FOR THE DEGREE OF MASTER OF SCIENCE.

Committee on Graduate Work

_____
David A. Randall

_____
Subhas Karan Venayagamoorthy

_____
Advisor: Eric D. Maloney

_____
Department Head: Richard H. Johnson

ABSTRACT OF THESIS

THE ROLE OF MOISTURE-CONVECTION FEEDBACKS IN SIMULATING THE INTRASEASONAL OSCILLATION

The sensitivity of the intraseasonal oscillation (ISO) in the National Center for Atmospheric Research's (NCAR) Community Atmosphere Model (CAM) version 3.1 with Relaxed Arakawa-Schubert (RAS) convection modified with the moisture trigger of Tokioka et al. (1988) is analyzed with respect to changes to the specified minimum entrainment rate. Implementation of the Tokioka moisture trigger results in a drier and cooler troposphere due to the suppression of deep convection. A higher minimum entrainment threshold leads to more suppressed deep convection and improves the sensitivity of convection to free tropospheric humidity. This is accompanied by enhanced intraseasonal variability in the tropics.

The simulated ISO which results from a non-zero minimum entrainment rate resembles a moisture mode. Variance of the column integrated saturation fraction is increased when minimum entrainment rate is increased, and precipitation becomes an increasingly non-linear function of saturation fraction which indicates that moisture-convection feedbacks are enhanced in the model. A reduction in the mean column moist static energy export by divergent motions indicates that the simulations with non-zero minimum entrainment thresholds are able to achieve negative gross moist stability which has been suggested as a necessary condition to be able to produce a moisture mode. This decrease in gross moist stability with increased minimum entrainment rate is accompanied by a lowering of the mean diabatic heating profile maximum.

Additional simulations are analyzed to investigate the impact of a rain re-evaporation fraction parameter on the simulated ISO. A higher rain re-evaporation fraction leads a stronger ISO signal in the model. However, In contrast to the effect of increased minimum entrainment rate, increased rain re-evaporation fraction yields a mean state which is warmer and moister. This discrepancy in mean state humidity change indicates that intraseasonal variability has no unique dependence on basic state humidity, in contradiction to that suggested in previous studies.

Walter Hannah
Department of Atmospheric Science
Colorado State University
Fort Collins, CO 80523
Fall 2009

ACKNOWLEDGMENT

This research would not have been possible without the support of many people. I would like to extend my deepest appreciation to my advisor, Dr. Eric D. Maloney, for his encouragement, guidance and invaluable assistance in helping me complete this work. I am also very grateful for the funding and opportunity to be work under his direction. I would also like to thank Dr. David Randall and Dr. Karan Venayagamoorthy for serving on my committee and reviewing my thesis. The support of the faculty and my peers at Colorado State University provided an exceptional and competitive environment for graduate studies. I would like to express immense appreciation for my friends who have helped make my time in Colorado very enjoyable. I would also like to thank my family above all for their constant encouragement and support. This work was supported by the Climate and Large-Scale Dynamics Program of the National Science Foundation under Grant ATM-0832868 and the Science and Technology Center for Multi-Scale Modeling of Atmospheric Processes, managed by Colorado State University under the cooperative agreement No. ATM-0425247. This work was also funded by award NA08OAR4320893 from the National Oceanic and Atmospheric Administration, U. S. Department of Commerce.

TABLE OF CONTENTS

THE ROLE OF MOSITURE-CONVECTION FEEDBACKS IN SIMULATING THE INTRASEASONAL OSCILLATION

1. INTRODUCTION

1.1. Background

1.1.1. Structure of the ISO

The Madden-Julian Oscillation (MJO), or Intraseasonal Oscillation (ISO) is a large-scale disturbance in tropical convection and the large-scale circulation with coherent signals in many other variables. The ISO was first noticed in the early 1970s (Madden and Julian, 1971, 1994, 2005) as a large spectral peak in upper and lower tropospheric winds, surface pressure and temperature. A large coherence in the cross-spectra between lower and upper tropospheric winds from rawinsonde data was also found which described an out of phase relationship. The large-scale circulation cell associated with this coherence in winds propagates eastward with typical phase speeds of 5 m s^{-1} and 10-15 m s^{-1} west and east of the date line, respectively. The period of the ISO varies from 30 to 90 days with a dominant spectral peak around 50 days (Zhang, 2005). Although the ISO generally can be described as being a planetary scale disturbance of wavenumber one to three in convection and precipitation, this phenomenon involves numerous multiscale processes.

An ISO event is considered to be occurring when an eastward moving center of anomalous deep convection is present over the equatorial Indian or West Pacific oceans with

areas of weak convection to its east and west. An event typically forms over the western Indian Ocean. The phase relationship between convection and upper level zonal wind continually shifts over the course of an event (Hendon and Salby 1994). As an event begins to amplify in the Indian Ocean convection tends to occur within upper level (above 200 hPa) westerly anomalies. As an event moves into the west Pacific the convective center tends to shift so that it lies within upper level easterlies. Lower level winds (850 hPa) have a similar structure and phase relationship as upper tropospheric winds, but with opposite sign.

The ISO features characteristics of a coupled phenomenon and a radiating response. During an ISO event the anomalous wind signature is similar to the Gill (1980) model forced with a heating anomaly on the equator (see also Sugiyama, 2009b). When coupled to convection, the circulation appears as a coupled Rossby-Kelvin wave which migrates eastward in tandem with anomalous convection at roughly 5 m s^{-1} in the eastern hemisphere. The Rossby wave response lies to the west of convection and consists of cyclonically rotating eddies at lower levels on either side of the equator. The Kelvin wave component of the coupled response sits to the east of the convective center and is symmetric about the equator. Although the convective signal is absent in the western hemisphere the dynamical signal is still present. The response in the western hemisphere is that of a Kelvin wave which propagates eastward at 10-15 m s^{-1} away from the area of Eastern hemisphere intraseasonal convective activity. The geographical distribution of the ISO Eastern hemisphere convective signal is accompanied by a corresponding signal in convergence at the surface which is not present in the western hemisphere. This highlights its role in amplifying intraseasonal convection in the eastern hemisphere (Salby and Hendon, 1994).

A fundamental characteristic of the ISO is that it exhibits strong seasonal variations in strength (Madden, 1986). A latitudinal migration between the Northern and Southern

hemispheres also exists. This seasonal migration of the ISO signal in low-level wind is present throughout the global tropics, with peak activity south of the equator during boreal winter and north of the equator during boreal summer (Salby and Hendon 1994). Although the broader tropical region has two peak seasons, overall ISO activity on the equator is much lower in the boreal summer months. A peak in intraseasonal variability has also been documented in the eastern Pacific warm pool during boreal summer (Maloney and Kiehl, 2002). This seasonal migration in latitude is stronger in the western pacific than in the Indian Ocean (Zhang and Dong, 2004).

The ISO has been shown to have significant interactions with the Asian and Australian monsoons. An amplification of the ISO can be observed prior to the summer onset of monsoon precipitation in both of these areas. It has also been found that the active and break period of the monsoons can be associated with ISO enhanced and suppressed phases. Another unique characteristic of the ISO is the northward propagation of individual intraseasonal convective events during boreal summer (Yasunari, 1979, 1980; Lawrence and Webster 2002). This northward propagation during boreal summer accompanies the eastward movement of the ISO that can be found in all seasons (Wheeler and Hendon, 2004). This additional poleward propagation of the ISO does not occur every year. Mehta and Krishnamurti (1988), for example, found regular poleward propagation in only half of the six years analyzed. In the southern hemisphere poleward propagation of individual events during austral summer is not prominent (Madden and Julian, 1994). The ISO has also been suggested to play a role in modulating precipitation during the North American monsoon (Lorenz and Hartmann, 2002).

The ISO has a significant impact on extreme events in the tropics and extratropics. For example, eastern Pacific tropical cyclone activity is related to the ISO. Maloney and Hartmann (2000) found that over twice as many tropical storms are generated during intraseasonal 850

hPa westerly phases than easterly phases of the ISO in the eastern Pacific during boreal summer. These storms that accompany the westerly phase also tend to be stronger than others during neutral or easterly phases. The westerly phase of the ISO supports favorable conditions for tropical cyclogenesis, such as highly cyclonic low-level relative vorticity and low vertical wind shear. Tropical cyclones are also modulated by the ISO in the Eastern hemisphere and the Atlantic (e.g. Camargo et al., 2009; Maloney and Shaman, 2008).

1.1.2. ISO Theory

Although observational studies of the ISO have provided a thorough description of its attributes, theoretical explanations of the underlying mechanisms that control its scale selection, vertical structure and propagation characteristics have been elusive (Wang, 2005; Tian et al., 2006). Early observational work by Madden and Julian (1971, 1972) on the ISO led to the idea that it could be explained by Kelvin wave dynamics, since these types of equatorial waves also propagate eastward and have a similar dynamical structure. However, dry versions of these waves propagate at 30-60 m s^{-1} for typical tropical static stability values, much too fast to explain the ISO. Chang (1977) proposed the idea that convectively coupled Kelvin waves may explain the ISO since these waves have slower propagation speeds due to Newtonian cooling and cumulus friction. The convective heating associated with these waves effectively reduces static stability which reduces a wave's phase speed as well. Although the western hemisphere response to the ISO can be explained by Kelvin waves (Hendon and Salby, 1996), the coupled disturbance of the eastern hemisphere ISO propagates slower than convectively coupled Kelvin waves which propagate at 10-15 m s^{-1}. Wheeler and Kiladis (1999) showed using the theoretical dispersion curves of Matsuno (1966) that outgoing longwave radiation (OLR) variance associated

with the ISO resides in a region of wavenumber-frequency space that is distinct from that of convectively coupled Kelvin waves.

A comprehensive theory of the ISO would need to account for an extensive list of its qualities. Such a theory would need to explain features such as a planetary scale circulation coupled with a large scale convective complex, a dominant spectral peak of around 50 days, a baroclinic circulation with boundary layer surface convergence leading the deep convective phase, slow eastward propagation in the eastern hemisphere with seasonally dependent poleward propagation, and a longitudinal dependent amplification and suppression of the convective signal (Wang, 2005). Due to the multi-scale nature of this phenomenon, considering the smaller scale structures of the associated convective complexes may be required to fully understand and predict the behavior of the ISO (Nakazawa, 1988).

Several theories have been proposed in the past few decades which attempt to explain the physical mechanisms that control ISO initiation, amplification and maintenance. These theories can be organized into five basic categories based on their key processes and feedback mechanisms: wave-CISK (Convective Instability of the Second Kind), surface evaporation feedback or wind-induced surface heat exchange (WISHE), stratiform instability, discharge-recharge, and moisture mode instability.

Wave-CISK theory involves instability that arises from cooperation between convective heating and large-scale, low-level convergence due to tropical wave processes (Hayashi, 1970; Lindzen, 1974). For CISK type instability, latent heat release and moisture convergence augment each other in a positive feedback in order to provide the energy needed to maintain the oscillation by conversion of CAPE (Convective Available Potential Energy) to large-scale motions. A consequence of the linear nature of wave-CISK is that it predicts increasing growth with higher wavenumber (Chao, 1995; Lim et al., 1990). This is in disagreement with observations which

show the ISO to be dominated by planetary scale features. CISK also requires that the atmosphere be conditionally unstable in the mean, whereas observations show that the tropical atmosphere is near-neutral to moist convective ascent (Emanuel, 1993).

Many Wave-CISK models produce an oscillation which has a much faster eastward propagation than the observed ISO. The propagation speed in these models seems to be dependent on the vertical profile of diabatic heating. Many studies have shown that specified heating profiles that contain a sufficient amount of the second vertical mode, in which lower and upper tropospheric heating and vertical velocity are out of phase, promote slower propagation speeds (Mapes, 2000). The ideal vertical heating profile that favors slow propagation remains in dispute. Some studies suggest that slower phase speeds require a reduction in static stability produced by heating which maximizes in the lower troposphere (Takahashi, 1987; Sui and Lau, 1989). On the other hand, studies such as Cho and Pendlebury (1997) suggest that top-heavy heating is a necessary condition to produce phase speeds characteristic of the ISO. These discrepancies suggest that pure wave-CISK theory cannot fully explain the ISO.

Modified wave-CISK theories have surfaced which aim to ameliorate the problem of wave-CISK instability collapsing to the smallest scales. These hypothesized modifications include the effects of surface friction on moisture convergence in the atmospheric boundary layer. This type of wave-CISK has been called the “frictional-CISK” or “frictional convergence” theory of the ISO (Wang, 1988). Frictional-CISK improves upon pure wave-CISK because wave induced moisture convergence by itself cannot result in sufficient instability at the largest scales. The instability resulting from frictional moisture convergence is supported by boundary layer convergence ahead of the free tropospheric wave convergence and the main convective disturbance.

There have been many observational studies which have documented frictional moisture convergence ahead of ISO convection (Jones and Weare, 1996; Maloney and Hartmann, 1998; Matthews, 2000). Maloney and Hartmann (1998) found that column integrated water vapor anomalies were strongly correlated with 1000 hPa convergence in the Indian and west Pacific oceans. They showed that the frictional moisture convergence which leads ISO convection, possibly in cooperation with shallow convection, helps to moisten the lower atmosphere and precondition the environment to be favorable for enhanced convective activity. Numerous other studies have also shown that boundary layer frictional moisture convergence is important to the ISO in general circulation models (GCM) (Kuma, 1994; Maloney, 2002; Waliser et al., 1999).

The wind-evaporation feedback or WISHE mechanism was proposed by Neelin et al. (1987) and Emanuel (1987). This theory states that waves which produce the ISO arise from an instability created from enhanced surface latent heat flux brought about by interactions of a wave's dynamic signature with the mean flow. Given the assumption of climatological easterlies, eastward propagating convective disturbances are maintained by enhanced surface evaporation from the ocean in regions of anomalous easterlies. These anomalous fluxes to the east of convection support subsequent convection there. The disturbance moves eastward as a result of the atmospheric warming which lowers the pressure ahead of the main trough. The WISHE mechanism has similar deficiencies to wave-CISK in that it favors short-wave growth and tends to produce propagation speeds that are too fast, although modeling studies such as Lin et al. (2000) have suggested that an evaporation-wind feedback mechanism may play a minor role in organizing ISO convection by reducing damping of midlatitude variability.

The WISHE mechanism relies on basic state easterlies to produce a zonal asymmetry in surface heat fluxes, yet observed mean winds are westerly in the equatorial Indian and west

Pacific oceans where the convective signal of the ISO is most active. Observational data from TOGA-COARE show that the phase relationship between ISO convection and enhanced evaporation is the opposite of Emanuel's (1987) prototype WISHE model in that large anomalous latent heat fluxes occur within the westerly phase of the ISO behind convection (Lin and Johnson, 1996). In spite of this weakness, non-linear forms of WISHE may still be an important for maintaining the ISO (Neelin et al., 1987; Xie et al., 1993; Wang and Li, 1994; Maloney and Sobel, 2004; Sobel et al., 2009).

Theories such as wave-CISK consider processes that include only the first baroclinic mode (i.e. a deep convective heating profile). Mapes (2000) proposed a theory that explicitly includes both the first and second baroclinic modes, which he termed "stratiform instability". The instability that arises is due to the interaction of the convective and stratiform heating structure (Houze, 1997; Mapes, 2000). Under this framework convectively coupled waves can organize from initial random noise when convective inhibition (CIN) fluctuations dominate that of CAPE. Given an initial tropospheric temperature anomaly with warmer air aloft and cooler air at lower levels which does not include the boundary layer, the frequency of deep convection is enhanced due to the reduction of CIN. This is followed at a lag by a stratiform heating over cooling profile similar to the initial temperature perturbation which generates eddy available potential energy due to a positive correlation of latent heating and temperature. In this manner a cycle of enhanced deep convective episodes in the form of an eastward propagating envelope is possible. Although the second baroclinic mode appears to be important to the structure of the ISO, the observed temperature profile associated with the onset of ISO convection is of the opposite polarity which suggests increased CAPE instead of reduced CIN (Benedict and Randall, 2007). Stratiform instability has also been used as a possible explanation of the dynamics in

equatorial waves such as Kelvin waves, but similar inconsistencies are apparent (Straub and Kiladis, 2003).

The discharge-recharge hypothesis was introduced by Bladé and Hartmann (1993) and works by gradually increasing instability through low-level diabatic heating and moistening which preconditions the atmosphere for deep convective episodes. The period of the ISO is then set by the recharge time for the instability. Kemball-Cook and Weare (2001) analyzed the onset of ISO convection with radiosonde data composites and suggested that the destabilization associated with the ISO is brought about by a combination of a low-level buildup of moist-static energy (MSE) and drying of the middle atmosphere due to subsidence from the wake of a previous ISO event. Other observational studies which have analyzed the vertical structure of the ISO (Sperber, 2003; Lin et al., 2004; Kiladis et al., 2005; Agudelo et al., 2006) have found that ISO deep convection was general preceded by low-level convergence and upward motion along with cooling and drying aloft. This results in a westward tilted vertical structure in time as low-level moisture is built up at low-levels and lofted into the upper troposphere during the deep convective phase of the ISO.

In a one-dimensional modeling study by Hu and Randall (1994) it was shown that interactions between radiation, convection and surface fluxes of moisture and sensible heat with fixed surface wind speed and without large scale dynamics resulted in an oscillating diabatic heat source with a period similar to the ISO. Radiative cooling aloft along with surface moisture fluxes tended to destabilize the atmosphere in their model.

Raymond (2001) showed a different way in which radiative feedbacks are important using an intermediate model in which radiative heating anomalies enhanced convection by reducing the effective static stability. He used the term radiative-convective instability to describe this mechanism. In order to quantify how much radiative heating can enhance diabatic

heating we can simply define an *enhancement factor* as the ratio between the column integrated radiative heating anomaly and the column integrated convective heating anomaly.

To continue the discussion of radiative-convective instability it is helpful to review the concept of gross moist stability. The gross moist stability (GMS) was originally formulated by Neelin and Held (1987) for a two layer model as the difference between the total dry static stability and gross moisture stratification, which is a measure of the amount of instability driven by lower level moisture convergence. GMS has been shown to explain the spatial pattern of large scale moisture convergence in the Tropics and has also been hypothesized to be important for the phase speed of the ISO (Neelin and Yu, 1994). The gross moist stability represents the net export of moist static energy (MSE) by divergent motions per unit mass flux in deep convective regions but can be thought of more simply as a measure of the net stability which includes the effects of moist convection. For the broader tropical region Yu et al. (1998) found the gross moist stability M to be positive but much smaller than the typical dry static stability. The reason for this is that M is a quantity resulting from cancellation of the gross dry stability by the gross moisture stratification M_q (Yu and Neelin, 1997). By formulating M in terms of M_s and M_q ($M = M_s - M_q$) we can see that with an increasing enhancement factor from high cloud induced radiational heating anomalies, and thus augmented gross moisture stratification, the gross moist stability goes to zero.

Based on the results of Yu et al. (1998), Lee et al. (2001) estimated that the necessary enhancement factor of radiative heating anomalies would need to be larger than 20% in order for the radiative-convective mechanism of Raymond (2001) to be effective at generating a slowly propagating eastward mode. Lin and Mapes (2004) analyzed the radiation budget of the ISO and found an enhancement factor of about 10-15% which falls short of the necessary value found by Lee et al. (2001), although Araligidad and Maloney (2008) suggested that by

considering other moist static energy sources such as surface latent heat flux this factor could be augmented over the 20% threshold. Raymond (2001) also pointed out that a key component to the model's oscillation was a built in inverse relationship between precipitation and the mean column saturation deficit, and the time lag between heavy precipitation and enhanced surface fluxes. The effects of surface fluxes were advected downstream into the region of deep convection. It can be argued that this lag causes a buildup of moisture in the column similar to the discharge-recharge theory of Bladé and Hartmann (1993), and could be responsible for setting the timescale of the simulated oscillation.

If a buildup of MSE is required in order to precondition the atmospheric column for a deep convective episode, then this suggests there should be a direct relationship between precipitation and the moisture content of the column. Bretherton et al. (2004) showed that this is indeed the case in the tropics by analyzing satellite based tropical rainfall and column water vapor estimates. They found a strong non-linear relationship specifically between rainfall and relative humidity (RH) in which rainfall increases rapidly when column integrated RH is greater than 70% which suggests the use of a critical value of a moisture related parameter is important for deep convection in the tropics (see also, Peters and Neelin, 2006).

Moisture mode instability theory can be traced back to Yu and Neelin's (1994) analysis of modes of tropical variability under convective adjustment. They referred to the mode that most resembles the ISO as the "propagating deep convective mode". Sobel et al. (2001) used the terminology "moisture waves" to refer to tropical disturbances that propagate perpendicular to the gradient of the background moisture field. Fuchs and Raymond (2007) applied the name "moisture mode" to the mode that most closely resembles the ISO in their model. Sugiyama (2009a) defines the moisture mode as a mode with a significant humidity signal in the free troposphere and whose dynamics exists under the balance described by the

weak temperature gradient approximation (WTG; Sobel et al., 2001) in which horizontal temperature gradients are negligible and diabatic heating is balanced by adiabatic cooling. In regions of weak tropical temperature gradients, moisture modes require strong moisture-convection feedbacks, such that the location of convection is determined by column humidity anomalies, and convective processes act to moisten the tropospheric column. These interactions are manifest as a strong relationship between tropical precipitation and preciptible water. Moisture mode instability also requires negative values of the effective GMS so that moisture anomalies can be built up in the free troposphere. Effective GMS incorporates MSE sources such as cloud radiative forcing and surface fluxes, in addition to export by divergent circulations (Sugiyama, 2009a). The results of Raymond and Fuchs (2009) suggest that moisture modes rely on a negative column integrated MSE export which corresponds to a negative GMS. However, GMS can effectively be negative if surface fluxes and radiative feedbacks can overcome MSE export by divergent circulations. Although moisture mode instability appears promising for explaining the ISO it is still unclear if this mechanism actually exists in nature. Other issues that demand further investigation are the requirement of negative, effective GMS and how this is achieved, as well as an explanation for the asymptotically constant growth rate at the small-scale limit.

1.1.3. Simulating the ISO

Producing realistic intraseasonal variability in a climate model has proven to be a difficult task. Early attempts at producing an ISO in models were encouraging because they were able to detect eastward propagating signals on intraseasonal time scales, however the propagation speeds were often found to be much faster than the observed ISO and closer to that of convectively coupled Kelvin waves (Hayashi and Sumi, 1986; Lau and Lau, 1986).

Following a limited intercomparison done by Park et al. (1990), a more comprehensive study by Slingo et al. (1996) compared numerous general circulation models (GCM) with respect to their intraseasonal variability and found that most models could not produce any significant eastward spectral power in the Tropics. Models which were able to produce eastward propagating signals were often plagued by signals which were too weak and phase speeds which were too fast. Many models also lacked any seasonality to the oscillation they produced. Later intercomparison studies found similar deficiencies (Sperber et al., 1997; Wu et al., 2002). On the other hand, more recent comparison studies have shown some improvement in model simulations of intraseasonal variability. In fact, certain models produce an ISO that is too strong or propagates too slowly (Zhang et al., 2006). A recent study by Kim et al. (2009) indicates that the use of new techniques of representing clouds in GCMs produce promising simulations of intraseasonal variability.

There have been many suggestions as to what factors are crucial for reproducing an accurate representation of the ISO in climate models. These include model resolution (e.g. Inness et al., 2001; Duffy et al., 2003), basic state (e.g. Inness et al., 2003), air-sea coupling (e.g. Waliser et al., 1999; Zheng et al., 2004; Sperber et al., 2005), and convective parameterization (e.g. Tokioka et al., 1988; Wang and Schlesinger, 1999; Maloney and Hartmann, 2001; Lee et al., 2003; Lin et al., 2005). Changes to convective parameterization are the most likely candidate for making major strides in ISO simulation since convection is central to the ISO and representing sub-grid scale processes in climate models can be done in a number of ways, many of them little constrained by observations. The most common way to quantify sub-grid scale processes in models is by parameterizing the bulk effects of these processes on the larger scale processes. Convective parameterizations are used to simulate the effects of an ensemble of convective

clouds as well as the resulting precipitation. Other cloud schemes are also usually included in models which simulate large scale precipitation.

A common method used to increase variance on intraseasonal time scales in climate models is to add a "convective trigger", which is designed to inhibit the growth of deep convection until a criterion is met. This is thought to allow the free troposphere to become conditioned through low level heating and moistening for an episode of more active deep convection as in the discharge-recharge hypothesis. Some convective triggers allow the convection scheme to be more sensitive to the environmental humidity. For some parameterizations deep convective clouds that reach the tropopause can occur in an anomalously dry environment because the clouds exhibit weak interactions with environmental air above the boundary layer (e.g. Derbyshire et al., 2004).

Tokioka et al. (1988) modified the convective scheme of Arakawa-Schubert (1974) with what is effectively a moisture trigger and showed that this improves model intraseasonal variability. In the Arakawa-Schubert (AS) scheme, clouds are spectrally divided into sub-ensembles, the heights of which are determined by the fractional entrainment rate. This method was based on the entraining plume concept which considers lateral entrainment being inversely proportional to the cloud's radius as the means by which the cloud is diluted and neutral buoyancy attained (see Simpson, 1971). In the original formulation of AS, entrainment rates of near zero are allowed, and it has been shown that allowing such weak entrainment produces little or no success at simulating a realistic ISO, depending on which model is used (Park et al., 1990). By adding a specified non-zero minimum entrainment rate, Tokioka et al. (1988) were able to suppress deep convection until the free troposphere became sufficiently moist for deep convection on intraseasonal time scales. Tokioka et al. (1988) implemented this parameterization into an aqua-planet version of the Meteorological Research Institute's AGCM

and obtained a robust 30-45 day oscillation in zonal wind, water vapor mixing-ratio, as well as other variables.

Itoh (1989) used an idealized nonlinear equatorial beta plane model with no land surface to investigate the scale selection of the ISO. Two versions of the model were used to also compare the effect of varying the convective parameterization. One model was implemented with the Kuo (1974) scheme with an added condition that relative humidity (RH) reach a critical value of 90% in order to initiate convection. A second model integration was considered in which the model treated convective heating and moisture implicitly with a CISK parameterization that assumed these variables to be proportional to low-level convergence only, and not moisture convergence as in the Kuo scheme. The CISK parameterization also included the same RH criterion of 90% for the onset of convection. Both of these methods were shown to produce an ISO-like feature and generally increase the variance on intraseasonal timescales in the model. Chao and Deng (1998) changed the cumulus scheme, without adding a convective trigger, within the Goddard Laboratory GCM configured as an aqua-planet and documented how this affected the ability to simulate an ISO. The three schemes used were the relaxed Arakawa-Schubert (RAS) scheme of Moorthi and Suarez (1992), a simple scheme from Chao and Lin (1994) and the moist convective adjustment scheme (MCA) of Manabe et al. (1965). In these simulations, the experiment with MCA was the most successful while RAS produced the least realistic intraseasonal variability. The results of these two studies show that successful simulation of the ISO will most likely be an emergent property of a model resulting from a number of different modifications and will not come simply from the addition of one simple parameter such as a convective trigger (Sobel et al., 2009).

Wang and Schlesinger (1999) tested three schemes in the University of Illinois Urbana-Champaign eleven layer GCM including the original Arakawa-Schubert (1974) scheme, the Kuo

(1974) scheme and the MCA scheme of Manabe et al. (1965). Each scheme was modified to change the RH constraint for convective heating to occur and was tested with various values of critical RH. This convective trigger allows moisture to accumulate such that a more restrictive threshold leads to greater variability similar to Tokioka et al. (1988). Wang and Schlesinger (1999) found that the simulated ISO was sensitive to the critical RH in all three cases but not very sensitive to which parameterization was used. The buildup of MSE caused by the RH criteria also resulted in a phase lag between condensational heating and moisture convergence. Previous studies have noted that this phase lag helps weaken short scale perturbations and hence allows for larger scale perturbations to become dominant. Although the models showed improved results with a more restrictive RH constraint, this came at the expense of increasingly unrealistic climatological winds. In all simulations increased critical RH resulted in weaker (stronger) tropical 200 hPa easterlies (westerlies).

Lee et al. (2003) confirmed the results of Wang and Schlesinger (1999) with aqua-planet simulations of the Seoul National University GCM. Lee used a simplified Arakawa-Schubert (SAS) (Numaguti et al., 1995) convection scheme similar to RAS. In some additional experiments they added the entrainment criterion of Tokioka et al. (1988) to SAS. They also implemented the MCA and Kuo schemes. They concluded that models with unconstrained convection schemes lack the ability to store and transport moisture, as evidenced by the fact that the precipitation patterns looked nearly identical to evaporation patterns. When no trigger is used in quasi-equilibrium closure schemes such as SAS or RAS a subset of convective plumes are allowed to form undiluted. This causes these models to exhibit a lack of strong variability in MSE and an unrealistically dry free troposphere in regions of high precipitation.

When the National Center for Atmospheric Research (NCAR) replaced their Community Climate Model 2 (CCM2) with the CCM3, the new model showed many improvements in its

overall climate simulation but the ISO was significantly degraded. Zhang and Mu (2005) noted that the likely factor for this was the use of the Zhang-McFarlane scheme (Zhang and McFarlane, 1995) in place of the Hack (1994) scheme. The Zhang-McFarlane scheme uses a CAPE based closure so that whenever the atmosphere is convectively unstable, convection is activated to remove the instability, but since the atmosphere in the tropics is usually found to be neutral or slightly unstable most of the time this causes the parameterization to activate convection at all times which leads to weak intraseaonal variability. Following the work of Zhang (2002), Zhang and Mu (2005) showed that modifying the scheme to have a different closure assumption based on CAPE generation by free tropospheric forcing allows for improved tropical intraseasonal variability. A RH threshold trigger of 80% was also added, similar to the methods of Wang and Schlesinger (1999). The addition of these modifications improved the ISO simulation in the CCM3, although discrepancies in the intraseasonal spectral peaks and spatial structure, relative to observations, were still evident.

Lin et al. (2008) expanded on the work of Wang and Schlesinger (1999) to study the effect of convective triggers on simulated convectively coupled equatorial waves as well as the ISO in the Seoul National University GCM. Lin used a version of the AS scheme, the Kuo scheme and a MCA scheme. They concluded that all wave modes were sensitive to the addition of a moisture trigger as well as the specific convective scheme. They found that as the strength of the trigger was increased, and convection more suppressed, variance of all wave modes was enhanced and the eastward propagation of the simulated ISO was improved. The MCA scheme produced larger variances, a more prominent spectral peak and a better eastward propagation of the ISO when compared to the other schemes. An interesting result of this research was to show that the strongest intraseasonal signal showed up in the model when no deep convection scheme was used. The reason for this is that without deep convection the large scale

condensation scheme is still contributing to precipitation and heating and is sensitive to the amount of moisture in the environment. This supports the notion that constraints which increase the sensitivity to free tropospheric moisture in deep convective schemes are important for improving simulated intraseasonal variability.

Maloney (2009) analyzed the intraseasonal moist static energy budget of a GCM that was modified to enhance the intraseasonal variability. The RAS convection scheme was used with an added Tokioka convective trigger and an additional parameter which specifies the amount of rain re-evaporation. The column integrated MSE budget was shown to be dominated by horizontal advection and the wind-driven component of surface latent heat flux. Fluctuations in eddy kinetic energy (EKE) were shown to strongly regulate the intraseasonal meridional moisture advection. During anomalous westerly phases enhanced synoptic-scale disturbances result in anomalously high EKE which caused drying of the lower troposphere through meridional advection. Subsequent suppression of synoptic-scale disturbance, and hence anomalously low EKE, during easterly anomalies allows for anomalous moistening of the free troposphere to occur. Latent heat flux anomalies act to oppose the effect of horizontal advection on the MSE tendency. This causes the recharge-discharge cycle of the simulated ISO to be much more gradual than if horizontal advection were acting alone. Maloney (2009) concluded that a realistic basic state equator to pole humidity gradient was essential for allowing the meridional advection to effectively contribute to the ISO signal in the model. This agrees with previous studies (Maloney and Hartmann, 2001; Inness et al., 2003) which state the importance of realistic distributions of basic-state variables in simulating an ISO.

Alternatives to conventional parameterization methods of representing sub-grid scale processes have been recently developed. One such method is the use of a multi-scale modeling framework (MMF; Khairoutdinov and Randall, 2001) or super-parameterization (SP), in which

small cloud resolving models are embedded in each grid cell of a GCM so that the statistics of sub-grid scale clouds can be more accurately estimated. Using this method in the National Center for Atmospheric Research (NCAR) Community Atmosphere Model (CAM) version 3.0 has been shown to produce a robust ISO (Thayer-Calder and Randall, 2009; Benedict and Randall, 2009). The SP-CAM does an excellent job of exhibiting the gradual vertical moistening and heating from the boundary layer up through the troposphere at intraseasonal timescales similar to observations. In spite of this improvement the ISO signal in the SP-CAM has several deficiencies. Overall the convective intensity associated with the ISO in the west Pacific is much stronger than observations. Some suggested causes of this are unrealistic boundary layer interactions, biases in the basic state and a lack of ocean coupling. The spatial distribution of the ISO signal in the MMF also has discrepancies such as a lack of weakening over the maritime continent. Unfortunately using an MMF comes at a much higher computational cost than conventional GCMs. Nevertheless, it is an important tool for expanding our understanding of the processes that regulate the ISO.

1.2. Why Studying the ISO is Important

Understanding the ISO is important for extended range forecasting and climate prediction because it affects many weather and climate phenomenon which have a direct impact on societies and economies around the world. Wet and dry phases of the ISO have been documented to influence the probability of extreme monsoon rainfall (Wheeler and Hendon, 2004) and are also involved in the annual onset of each monsoon period (Yasunari, 1979; Hung and Yanai, 2004). The formation of tropical cyclones is favored in regions of the westerly phase of the ISO (Liebmann et al., 1994; Maloney and Hartmann, 2000; Mo, 2000). The El Niño-Southern Oscillation (ENSO) appears to modulate ISO activity from year to year (Lau and Chan,

1986). There is also evidence that ISO events can trigger as well as kill an El Niño event by exciting oceanic Kelvin waves (Takayabu, et al., 1999; Bergman et al., 2001). Being able to simulate the effect of these tropical features in climate models is essential for accurate climate forecasting and therefore an accurate simulation of the ISO is likely to improve predictive skill at these long timescales. Outside of the tropics the influence of the ISO can be linked to extra-tropical weather. ISO convection has been shown to have a strong coherence to extra-tropical wave-trains (Lau and Phillips, 1986). These so-called teleconnections can impact mid-latitude circulations and precipitation (Higgins and Mo, 1997; Higgins et al., 2000).

It has been notoriously difficult to simulate the ISO as well as other convectively coupled processes on a variety of timescales in models. Improving models' ability to generate realistic tropical variability will have far reaching implications.

1.3. Overview of Study

This thesis is a study to analyze the sensitivity of the NCAR Community Atmosphere Model (CAM) version 3.1 with Relaxed Arakawa-Schubert (RAS) convection to changes in a minimum entrainment rate parameter with respect to its ability to produce a robust intraseasonal oscillation (ISO).

Chapter two provides detailed descriptions of how the model integrations were configured as well as the observational datasets used for comparison. This section also outlines the methods utilized in the sections to follow. Chapter three investigates aspects of the mean state and intraseasonal variability of the model. This section uses the simulation diagnostic methods presented by the CLIVAR MJO working group (see Kim et al., 2009) to evaluate the changes to the intraseasonal variability of the model when a non-zero minimum entrainment is employed. Chapter four presents process oriented diagnostics which focus on the role of key

processes which may be responsible for dictating the response of the model to varying the minimum entrainment rate parameter within RAS. Additional model integrations are analyzed which highlight the influence of a rain re-evaporation fraction parameter on the simulated ISO. Summary and discussion are presented in chapter five.

2. DATA AND METHODOLOGY

2.1. Data

2.1.1. NCAR-CAM Simulations

The National Center for Atmospheric Research (NCAR) Community Atmosphere Model (CAM) version 3.1 (CAM3, Collins et al., 2006) is used for this study. CAM3 is the atmospheric component of the Community Climate System Model version 3. The Relaxed Arakawa-Schubert (RAS) convective parameterization of Moorthi and Suarez (1992) is used in place of the standard Zhang-McFarlane (1995) scheme to improve the models tropical intraseasonal variability as in previous modeling studies (Maloney and Sobel, 2004; Maloney, 2009). The version of RAS used in this study initiates convection from the lowest model level. The Hack (1994) scheme which is also used in the standard setup of CAM3 is included to simulate shallow convection.

RAS simplifies some of the calculations made in the original Arakawa-Schubert (AS; 1974) scheme so that it is more economical. Instead of requiring the cloud ensembles to reach quasi-equilibrium as in AS, RAS simply relaxes the state towards equilibrium each time the parameterization is invoked. The convective adjustment of RAS is governed by a cloud work function which is strongly regulated by boundary layer moist static energy (MSE). Although RAS is sensitive to the amount of moisture in the boundary layer, the standard version of this scheme is relatively insensitive to the amount of moisture in the free troposphere. The reason for this is that cloud ensemble members in RAS limit their entrainment in order to buffer themselves from a dry free tropospheric environment. Thus, the version of RAS used in this study has been modified to include a minimum entrainment parameter similar to the method

used by Tokioka et al. (1988) to address this issue. Cloud ensemble members that entrain less dry air than the prescribed minimum entrainment are suppressed with this modification. In this way we can make the convective parameterization sensitive to the amount of moisture in the free troposphere and have some control over the strength of the consequential suppression of deep convection

In Tokioka et al. (1988) the prescribed minimum entrainment (μ_{min}) was related to the sounding-dependent depth of the boundary layer, such that $\mu_{min} = \alpha/D$ (where α is a dimensionless constant and D is the depth of the boundary layer). Using this method resulted in an enhanced ISO signal in their model, although the reasons for this enhancement were not explained in detail. The version of RAS used here assumes a constant boundary layer depth of D = 2000 when calculating μ_{min} so that the minimum entrainment parameter is fixed for each model run. Results based on this assumption should not significantly differ from that of Tokioka (1988) since the analysis presented here focuses on the Tropics where temperature gradients are weak and the temporal variability of boundary layer MSE is small. As will be shown below, intraseasonal variability in the CAM3 with RAS convection is strongly related to the minimum entrainment threshold.

This version of RAS also allows a specified fraction ε of convective precipitation to be exposed to environmental air and evaporated depending on the environmental relative humidity, temperature and pressure as well as microphysical assumptions such as droplet size distribution and fall velocities (e.g., Sud and Molod, 1988). Previous studies have shown that simulated intraseasonal variability is sensitive to changes of this parameter (e.g. Maloney and Hartmann, 2001). Although convective rain re-evaporation in this parameterization is not allowed to explicitly generate subgrid-scale downdrafts, it is likely to have impacts on the grid cell vertical velocity through modifications to the vertical heating structure. Previous studies

have shown that parameterizations of rain re-evaporation lead to enhanced moisture convection feedbacks in models (e.g. Grabowski and Moncrieff, 2004).

Four different sixteen year simulations of CAM3 with the RAS convective scheme discussed above were conducted. The primary simulations analyzed were configured with ε = 0.3 and α = 0.0, 0.2, 0.4 and 0.6. Two additional simulations were analyzed in section 4.3 in which α was held fixed at α = 0.2 and ε varied from 0.05 to 0.6. Simulations are integrated using a spectral dynamical core at T42 resolution (approximately 2.8° x 2.8° grid resolution) with climatological seasonal cycles of sea surface temperatures and solar insolation. Twenty six levels are resolved in the vertical and the model time step is twenty minutes.

2.1.2. Observational Data

The European Center for Medium-Range Weather Forecasts (ECMWF) interim reanalysis product (ERAi; Simmons et al., 2007) is used throughout this study as a resource for comparison of atmospheric variables and was provided by ECMWF and obtained from the ECMWF data server. Reanalysis data provides comprehensive spatial coverage for the area of interest where observations are sparse which makes it ideal for this type of research. The ERAi dataset has a 1.5° x 1.5° horizontal resolution and thirty seven available vertical levels. A subset of this dataset is used here which includes thirteen vertical levels from 975 to 100 hPa, latitudes between 15° N and 15° S and all longitudes. A fifteen year time period was used which extends from January 1^{rst}, 1990 to December 31^{rst}, 2004. ECMWF 40-year reanalysis (ERA40, Uppala et al., 2005) was also used for comparison since the ERAi dataset is new and not as familiar as ERA40. ERA40 has a 2.5° x 2.5° horizontal resolution and was only used in the tropical belt from approximately 10° N to 10° S for a 12 year time period from January 1^{rst}, 1990 to December 31^{rst}, 2001. Tropical precipitation data was used from the Tropical Rainfall Measuring Mission (TRMM) gridded 3b42

product for five years worth of data from 1998-2002. In the cases in which TRMM data did not cover a sufficient time period the Climate Prediction Center (CPC) merged analysis of precipitation (CMAP, Xie and Arkin, 1997) enhanced data was used for the period covered by the ERAi data. Special Sensor Microwave Imager (SSM/I) version 6 precipitation and column water vapor data was also used in this study to examine the relationship between column precipitable water and precipitation. SSM/I data was acquired from Remote Sensing Systems (http://www.remss.com/; Wentz and Spencer, 1998).

2.2. Methodology

2.2.1. Filtering

Intraseasonal anomalies for all data are isolated by applying a linear non-recursive digital bandpass filter with half power points at 30 and 90 day periods. The frequency response of the filter retains nearly full power at 40-50 day timescales which is the dominant timescale of the ISO as documented in observations of zonal wind (Madden and Julian, 1971). Each of the two filters which make up the bandpass filter are constructed with fifty nine weights so that one hundred eighteen values are lost from the ends of the time series during filtering. Lanzcos smoothing was applied to the weights.

2.2.2. Composites

Composites were constructed by two methods, one which uses an empirical orthogonal function (EOF) based index and another using a simple filtered 850 hPa zonal wind index. The EOF index was determined from filtered 850 hPa zonal wind data averaged from approximately 10N – 10S depending on the resolution of the data under consideration. EOFs were calculated on this equatorial averaged data for all seasons of the record. Although complex EOF (CEOF)

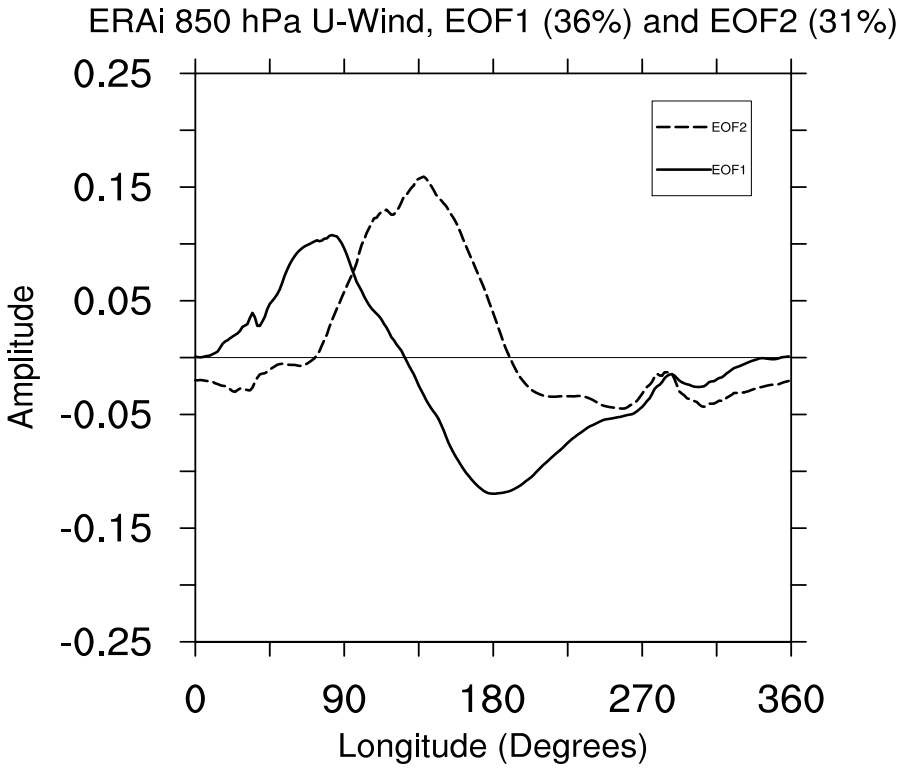

Figure 2.1. EOF1 and EOF2 of the equatorial averaged (10.5°N – 10.5°S) filtered 850 hPa zonal wind data for ERAi.

analysis can be used to better identify the propagation characteristics of intraseasonal anomalies, the main purpose of the EOF index used here is to identify events, and is approximately equivalent to EOF analysis for a narrow band propagating signal. For the purposes of this study either of these methods would produce similar results. The two leading EOFs derived from observations are shown in Figure 2.1 and explain a total of 67.4% of the intraseasonal zonal wind variance. To construct the index the amplitude and phase of the two leading principle components (PCs) were calculated from equations 2.1 and 2.2, similar to the methods of Wheeler and Hendon (2004).

$$Amplitude = \sqrt{PC1^2 + PC2^2} \qquad (2.1)$$

$$Phase = \arctan\left(\frac{PC1}{PC2}\right) \qquad (2.2)$$

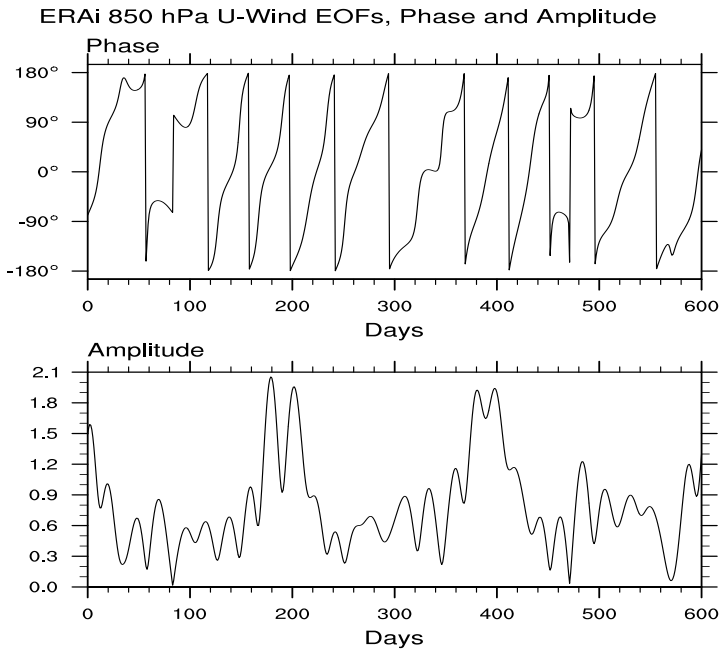

Figure 2.2. EOF1 and EOF2 of the equatorial averaged (10.5°N – 10.5°S) filtered 850 hPa zonal wind data for ERAi.

The method used here only differs from Wheeler and Hendon (2004) in that they use a multivariate EOF analysis on 850 and 200 hPa zonal winds and outgoing longwave radiation, whereas the method used here uses only 850 hPa zonal wind. Given the strong coherent variability of the ISO, these methods produce similar results. A snapshot of this index in phase and amplitude is shown in Figure 2.2 using the ERAi dataset. The phase of the index indicates an approximate spatial state of the anomalous wind field associated with an intraseasonal disturbance while the amplitude gives an approximate measure of the strength of the anomaly. ISO events were selected by isolating periods in which the amplitude is greater than one standard deviation from zero. These events were then composited by binning the events into eight phases, each of which corresponds to 45° of phase angle.

An alternative index was created to facilitate time vs. height composites at specified longitudes. For a given longitude this index was created by finding days in which the filtered equatorial averaged 850 hPa zonal wind at that longitude had a maximum exceeding one

standard deviation from zero. Composites were then constructed as a function of lag relative to these maxima. Events were selected so that they occurred at least twenty days after the previous event.

3. Model Variability

3.1. Diagnostics of Intraseasonal Variability

The sensitivity of the of NCAR's Community Atmosphere Model (CAM) with Relaxed Arakawa-Schubert (RAS) convection is examined with respect to changes in the minimum entrainment parameter. In this section the model's intraseasonal variability is diagnosed and compared with that of observational data. The following analysis provides justification for the inclusion of minimum entrainment thresholds for enhancing intraseasonal variability in climate models, and provides consistency with previous studies (e.g. Tokioka et al., 1988; Wang and Schlesinger, 1999)

3.1.1. Mean State

Mean boreal winter (November-April) 850 hPa zonal winds are shown in the left panel of Figure 3.1 for all model runs and ERAi data. In all plots, low level easterlies prevail throughout most of the Tropics. An area of westerly wind exists over central Africa which is stronger in the model than observed. Much of the equatorial Indo-Pacific region can be characterized by westerlies in observations. This feature is partially captured by the model, although there are discrepancies as to the spatial distribution and amplitude. This region of westerly wind in the model has a larger meridional span which extends farther south than in observations. This region also has a smaller zonal extent in the model with weak easterlies over the Indian Ocean where observations show mean westerlies. If the ISO can be appropriately described as a moisture mode then this discrepancy will likely be important to the ISO structure since the

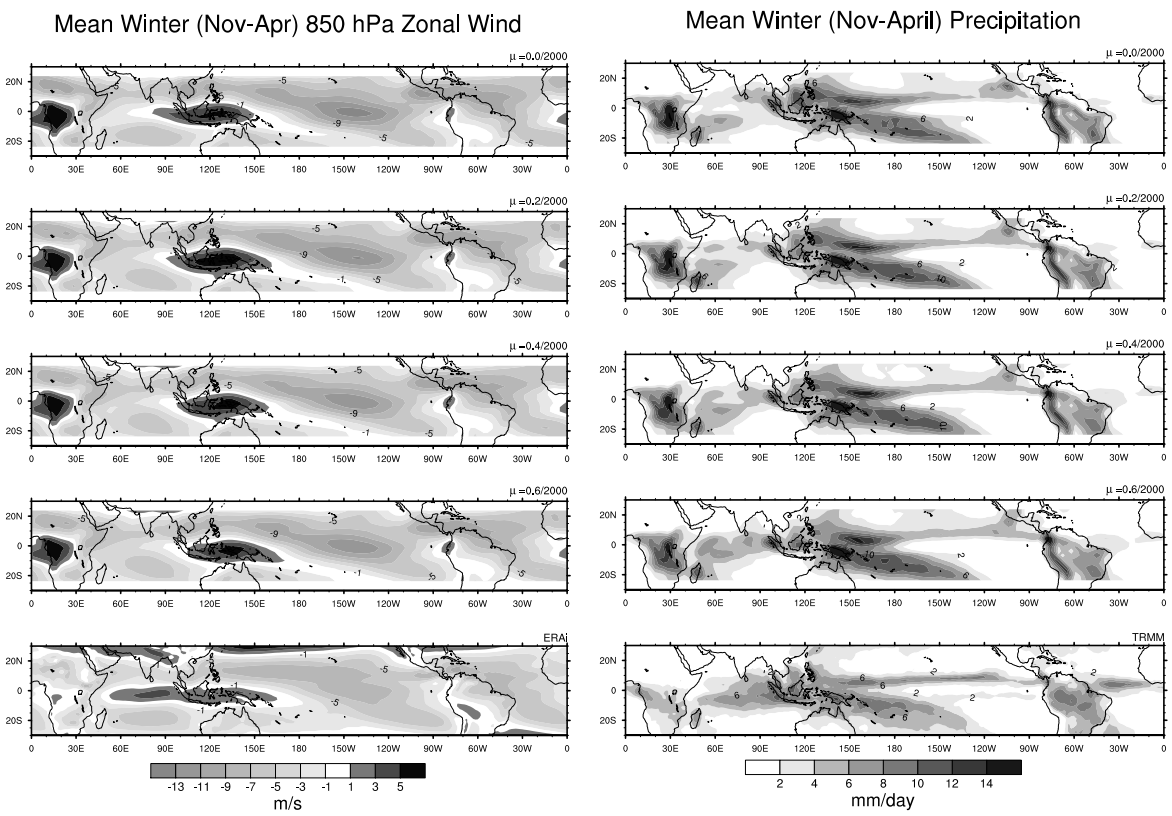

Figure 3.1. November-April mean 850 hPa winds (left panel) and precipitation (right panel) for model runs α = 0.0, 0.2, 0.4 and 0.6 and ERAi data. Units are m s^{-1} for 850 hPa wind and mm day^{-1} for precipitation.

propagation of moisture modes is thought to be partially controlled by eastward moisture advection. Although the amplitudes of the mean winds are comparable among runs, the spatial distribution tends to shift eastward with increasing minimum entrainment parameter. Degradations of the mean state in other studies employing moisture triggers has been noted, including the response to critical relative humidity threshold found by Wang and Schlesinger (1999) in which they noted that upper level winds become less realistic as a moisture trigger is increased.

Mean boreal winter precipitation has similar amplitude biases (Fig. 3.1, right column). Some areas in the model tend to have much higher mean precipitation than observations, while the Indian Ocean tends to have too little precipitation. These issues are somewhat corrected

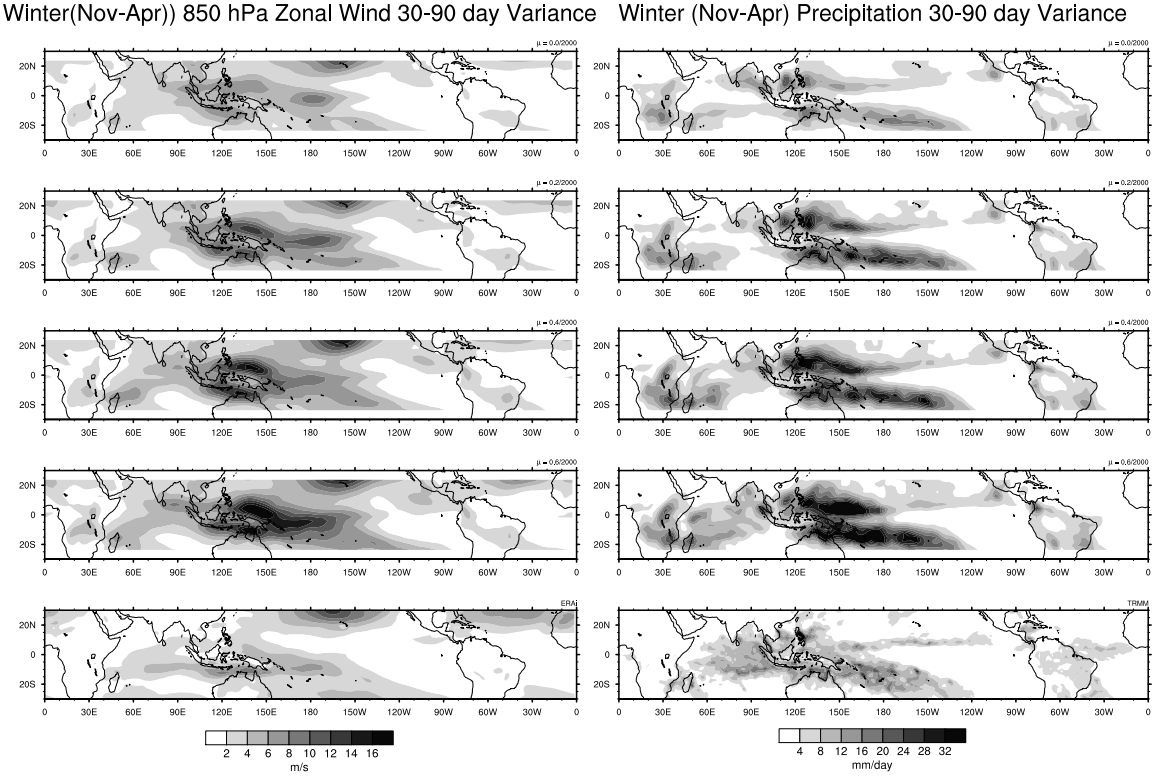

Figure 3.2. November-April 30-90 day variance for 850 hPa winds (left panel) and precipitation (right panel) for model runs α = 0.0, 0.2, 0.4 and 0.6 and TRMM data. Units are $m^2\ s^{-2}$ for 850 hPa wind and $mm^2\ day^{-2}$ for precipitation.

when the minimum entrainment parameter is increased, resulting in more precipitation in the Indian Ocean and less over parts of the Maritime continent. The strong precipitation and low-level wind bias over central Africa is also slightly reduced.

3.1.2. Distribution of Variance

The left panel of Figure 3.2 shows the intraseasonal zonal wind variance for each model integration and ERAi for boreal winter. In all cases tropical variance maximizes over the ocean surface in the west Pacific and somewhat in the Indian Ocean. Relatively low variance is found over the land masses of the maritime continent consistent with observations. Model variance generally increases with increasing minimum entrainment rate with no significant changes to

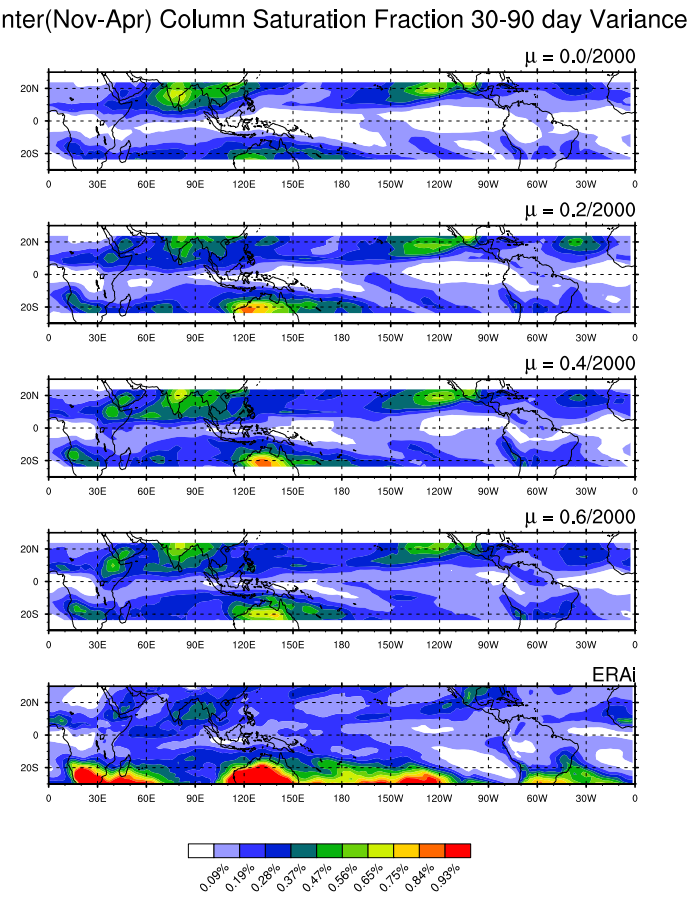

Figure 3.3. Winter (Nov-Apr) 30-90 day saturation fraction variance for model runs α = 0.0, 0.2, 0.4 and 0.6 and ERAi data.

the spatial pattern. Intraseasonal low-level wind variance is overestimated over much of the Indo-Pacific region in all model configurations. The spatial distribution broadly resembles observations, but Northern Hemisphere variance is too high relative to that in the Southern Hemisphere. Similar results can be found when using all-season or boreal summer data.

Winter precipitation variance for filtered data is shown in the right column of Figure 3.2 for each model run and five years of TRMM data spanning from 1998 through 2001. The model exhibits regions of high variance that straddle the equator similar to observations. Intraseasonal precipitation variance is shown to increase in all areas of the Tropics when the minimum entrainment parameter is increased. Similar to intraseasonal low-level wind variance,

intraseasonal precipitation variance becomes stronger than observations with non-zero minimum entrainment thresholds.

If the model's intraseasonal variability is in fact driven by moisture mode instability and characterized by a strong relationship between precipitation and water vapor then there should be a detectable change in how the model simulates the variability of the moisture in the column. To investigate this, the variance of 30-90 day bandpass filtered column saturation fraction was computed for each model run as well as ERAi (Fig. 3.3). The saturation fraction was calculated as the ratio of the column integrated specific humidity to the column integrated saturation specific humidity. Unlike zonal wind and precipitation variance, model variance of saturation fraction is generally lower than that found in observations. In the model with no minimum entrainment constraint we can see an area of very low variance in the Indo-Pacific region which interestingly corresponds to regions of high zonal wind and precipitation variance. An increase of intraseasonal saturation fraction variance occurs in this region with increasing minimum entrainment rate, which appears to converge towards the pattern found in observations (Fig. 3.3, bottom panel). This could be due to the model's increasing ability to build up and transport moisture, possibly as a direct result of the Tokioka trigger limiting the occurrence of deep convection. Higher baroclinic modes such as that associated with shallow convection and stratiform heating (Mapes, 2000; Peters and Bretherton, 2006) may be enhanced and contribute to moistening when deep convection is suppressed. Horizontal advection may also act as an important moistening agent in advance of the deepest convection (e.g. Maloney, 2009; Maloney et al., 2009).

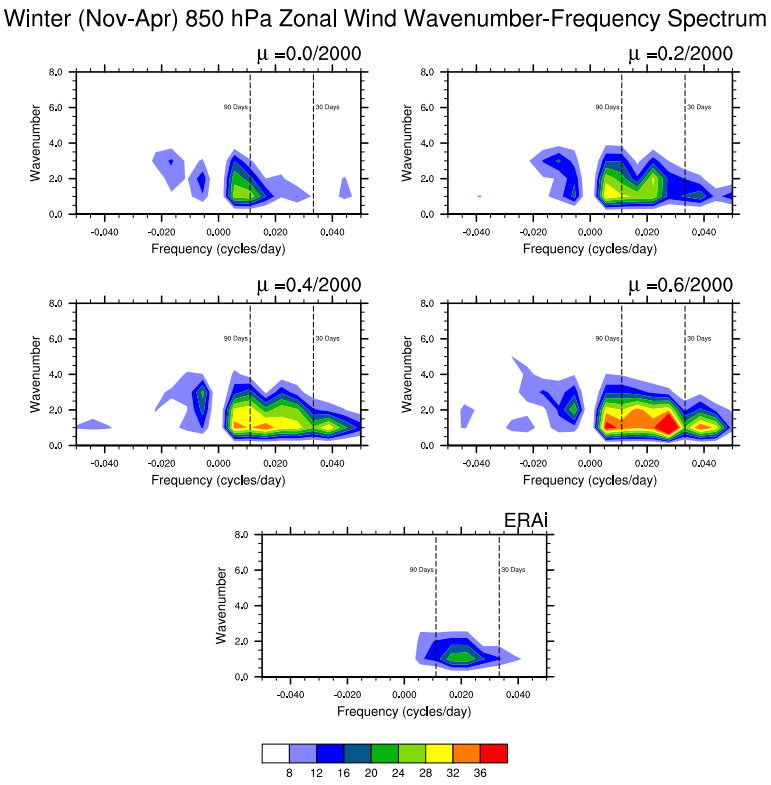

Figure 3.4. Winter (Nov-Apr) zonal wind wavenumber-frequency spectra for model runs α = 0.0, 0.2, 0.4 and 0.6 and ERAi data. Spectra were calculated from equatorially averaged data from approximately 10S – 10N. Positive frequency indicates eastward propagating signals, while negative indicates westward propagating signals.

3.1.3. Space-Time Spectral Analysis

Boreal winter wavenumber-frequency spectra of equatorial averaged 850 hPa zonal winds are shown in Figure 3.4 with thirty and ninety day periods highlighted by dashed lines. Observations show a focused spectral peak around eastward propagating fifty day periods and wavenumber one. Without the Tokioka moisture trigger, model wind variance is weaker than observed in the eastward thirty to ninety day band and wavenumbers one through three. Model spectra show increasing variance in the ISO band with increasing minimum entrainment parameter. Model spectra have the highest power at eastward wavenumber one, similar to observations, but in all model spectra westward power is too strong. As compared to observations, model variance is also too high at higher wavenumbers and lacks a single

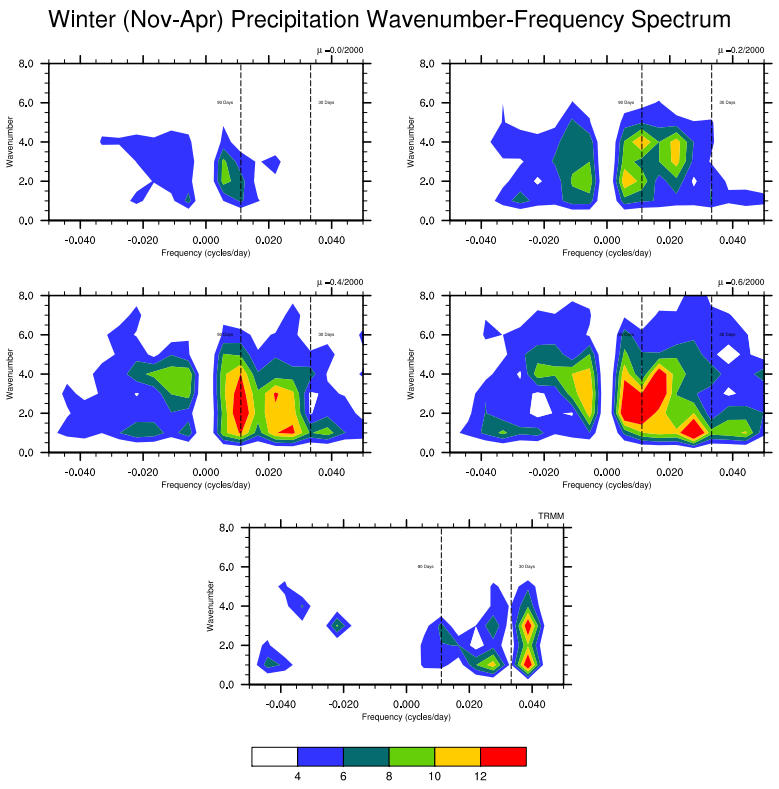

Figure 3.5. Winter (Nov-Apr) precipitation wavenumber-frequency spectra for model runs α = 0.0, 0.2, 0.4 and 0.6 and ERAi data. Spectra were calculated from equatorially averaged data from approximately 10S – 10N.

dominant peak. Similar results can be found by comparing summer or all-season spectra (not shown). This model exhibits strong regulation of eastward propagation by horizontal advection (Maloney et al., 2009), and thus strong fluctuations in background steering currents caused by excessive wind variance in the tropics may cause a lack of localization to a dominant propagation speed and period.

Precipitation wavenumber-frequency spectra are shown in Figure 3.5 for all model configurations and TRMM data. The spectrum calculated from TRMM data shows the highest power outside of the ISO band with a peak around twenty five days. Peak spectral power within the ISO band occurs around forty days. Compared to zonal wind spectrum, precipitation has more variance at higher wavenumbers as well as more westward power relative to eastward

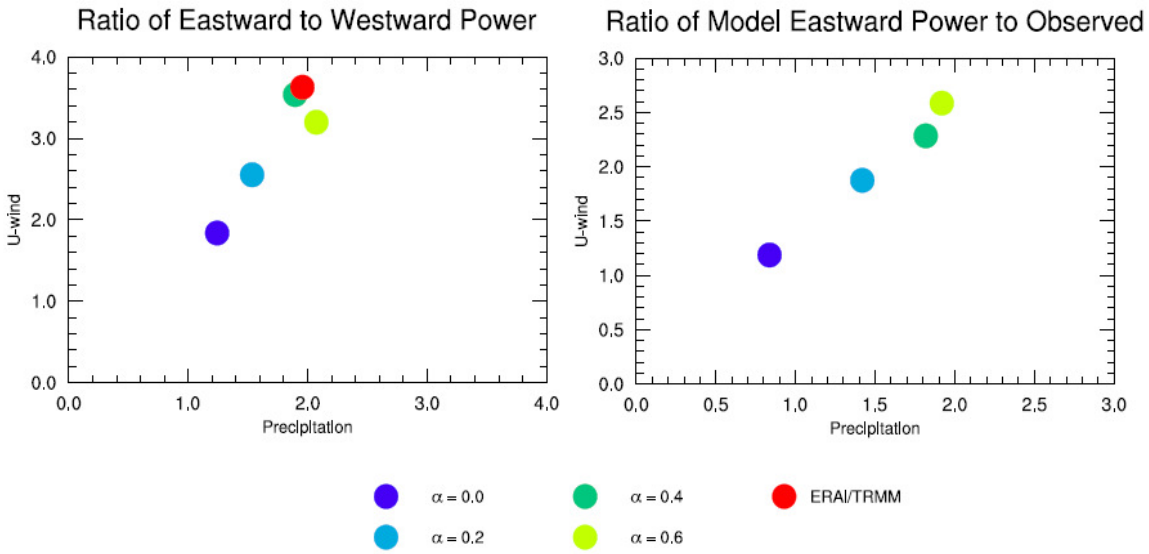

Figure 3.6. Winter (Nov-Apr) precipitation wavenumber-frequency spectra for model runs α = 0.0, 0.2, 0.4 and 0.6 and ERAi data. Spectra were calculated from equatorially averaged data from approximately 10S – 10N.

power. As was shown in the zonal wind spectra (Fig. 3.4), precipitation variance in the ISO band increases as the minimum entrainment parameter is increased.

The change in ISO band spectral power between each model run is perhaps best characterized by Figure 3.6. The left panel shows a scatter plot describing the ratio of eastward spectral power in the ISO band to its westward counterpart for all model runs and observations. The precipitation ratio is shown on the abscissa and the zonal wind ratio is on the ordinate. This ratio was computed by integrating the spectral power between thirty and ninety day periods and wavenumbers one through four. Variance appears to converge towards that of observations in both zonal wind and precipitation. The similarity of the ratios for $\alpha = 0.4$ and $\alpha = 0.6$ seems to indicate that the effect of the Tokioka moisture trigger saturates at high thresholds. The right panel shows the ratio of model eastward power to observed eastward power within the same

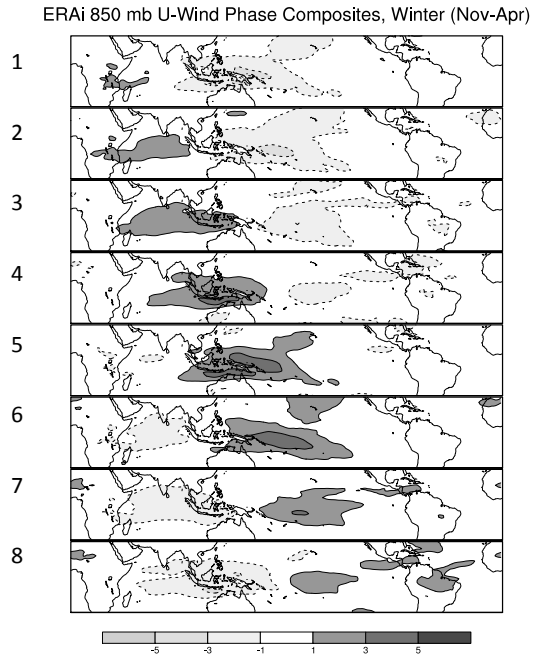

Figure 3.7. Winter (Nov-Apr) 30-90 day filtered zonal wind composites for ERAi data. Composites were created from an ISO index based on EOF analysis of filtered zonal wind data. Phase numbers are indicated on the left side of the plots.

spectral region for both zonal wind and precipitation. This figure illustrates the exaggerated intraseasonal variability by the model in both variables.

3.2. Composite Structure

In this section the effect of increasing the minimum entrainment parameter on the composite structure of the simulated ISO is analyzed. The resulting horizontal and vertical structure will then be compared to that of observations. This analysis aims to uncover the possible mechanisms responsible for the increase in intraseasonal variability with higher minimum entrainment rates shown in section 3.1.

3.2.1. EOF Based Composites

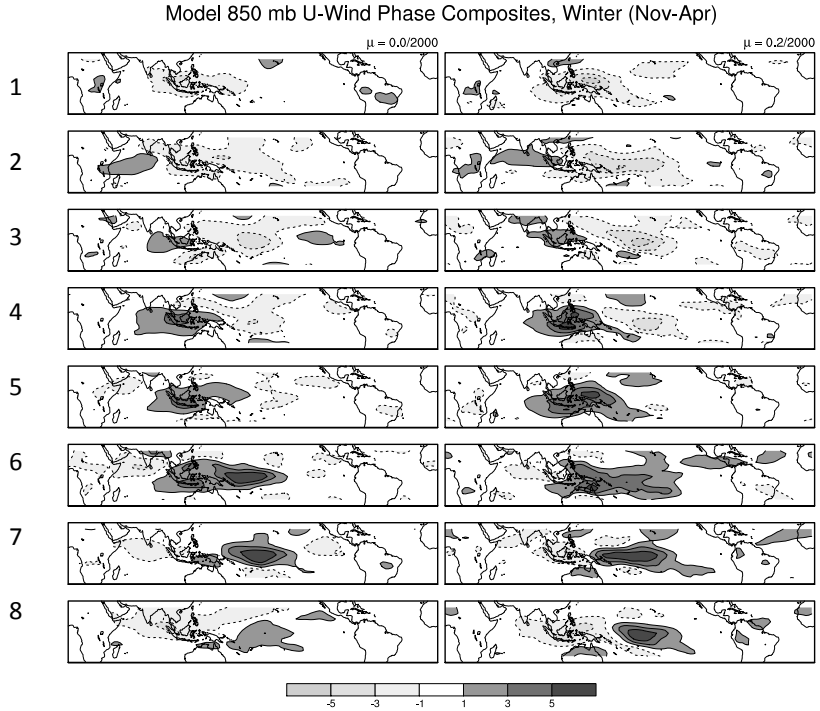

Figure 3.8. Winter (Nov-Apr) 30-90 day filtered zonal wind composites from model runs with $\alpha = 0.0$ (left column) and $\alpha = 0.2$ (right column). Composites were created from an ISO index based on EOF analysis of filtered zonal wind data. Phase numbers are indicated on the left side of the plots.

Composites shown in this section were created from an EOF based index of thirty to ninety day equatorially averaged zonal wind data as described in section 2.2.2. After events were selected and the appropriate phases determined, maps of filtered data from these events were averaged to produce composites. ERAi 850 hPa zonal wind composites are shown for boreal winter (Nov-Apr) in Figure 3.7 separated into eight phases with Phase 1 shown in the top panel. Phase 1 represents the birth of an ISO event with anomalous easterlies over the Maritime continent and a smaller region of weak anomalous westerlies in the western equatorial Indian Ocean to the north of Madagascar. Subsequent phases show these anomalies propagating eastward in tandem. Easterly anomalies that lie to the east of anomalous westerlies begin to decay at Phase 3 and are no longer noticeable by Phase 5. Westerly anomalies peak at Phases 5 and 6 and are evident in all phases, although these are weak and less organized at Phases 7 and 8 when the anomalies reach the dateline.

Figure 3.8 shows similar phase composites for the model runs with $\alpha = 0.0$ (left column) and $\alpha = 0.2$ (right column). Propagation in the $\alpha = 0.0$ run looks notably weak compared to that in observations, although localized regions of high amplitude wind anomalies occur. The simulated ISO appears to be almost stationary for Phases 2 through 4 as well as 5 through 8. This poor eastward propagation is exposed in more detail in Figure 3.10 below. Regions of anomalous easterlies are displaced slightly northward compared to the corresponding phases in observations. Westerlies anomalies also lack a realistic southward extent. Phases 3 and 4 also show regions of anomalous westerlies that do not have corresponding features in observations, such as the extra tropics of the central pacific, and in the equatorial eastern Pacific. The amplitude of anomalous westerlies in all phases is similar to observed, except for Phases 6 and 7 in which the amplitude of the westerly winds are too strong. Easterly amplitudes compare more favorably in all phases.

The right column of Figure 3.8 shows the phase composite of the model run with $\alpha = 0.2$. The ISO structure in this model shows some slight improvements over the $\alpha = 0.0$ run. A more realistic southward extent of westerly anomalies is evident in Phases 4 through 6. The spatial structure of easterly anomalies appear relatively more organized compared to the previous run and features such as the easterly anomalies over the maritime continent in Phase 8 more closely resemble that of observations. Westerly anomalies also do not exhibit the same quasi-stationary behavior between some phases as is seen in the $\alpha = 0.0$ simulation. The amplitude of anomalous wind is higher than that of observations as well as that of the $\alpha = 0.0$ run.

Further improvements are seen in zonal wind composites of model runs with $\alpha = 0.4$ and $\alpha = 0.6$ (Fig. 3.9). As the characteristics of the simulated ISO's propagation become more like observations, the amplitude of anomalous winds becomes too strong, particularly over the west

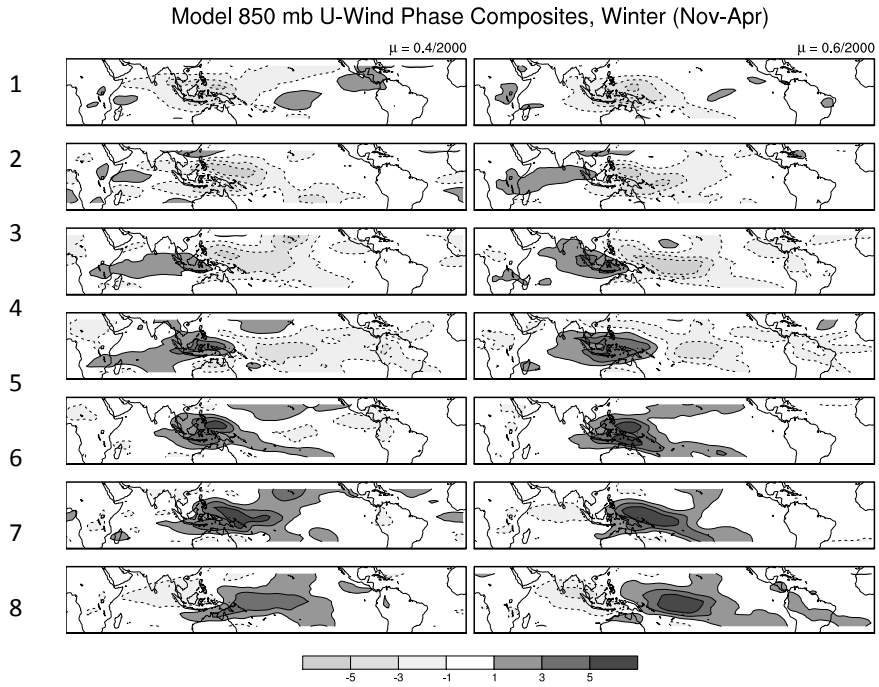

Figure 3.9. Winter (Nov-Apr) 30-90 day filtered zonal wind composites from model runs with $\alpha = 0.4$ (left column) and $\alpha = 0.6$ (right column). Composites were created from an ISO index based on EOF analysis of filtered zonal wind data. Phase numbers are indicated on the left side of the plots.

Pacific. Anomalies also tend to have a larger zonal and meridional extent. Some interesting differences between these composites suggest that the response of increasing the minimum entrainment parameter is not linear. By comparing phase 8 between the composites for $\alpha = 0.2$, $\alpha = 0.4$ and $\alpha = 0.6$ we can see that the anomalous westerlies become weaker but cover a larger area from $\alpha = 0.2$ to $\alpha = 0.4$, but then become stronger again without much change to their spatial extent from $\alpha = 0.4$ to $\alpha = 0.6$. However, some of this variability may not be statistically significant.

3.2.2. Lag Composites

An alternate view of the composite structure is shown in Figure 3.10 in which composites were constructed using a filtered zonal wind index based at 155° E. Lag in days relative to the maximum zonal wind is shown on the ordinate and longitude is shown on the

abscissa. Zonal wind is shown in colors and precipitation in contours with negative contours dashed. Note that CMAP precipitation was used in order to cover the same time period as that of the ERAi data used here. Composites based on observations indicate an average phase speed of approximately 8 m s^{-1} for intraseasonal westerly anomalies between 90° E and 180° E (Fig. 3.10, lower panel). The phase speed increases past the dateline to approximately 25-30 m s^{-1}. The phase relationship between zonal wind and precipitation displays a similar quadrature relationship to the results of previous observational studies (e.g. Hendon and Salby, 1994). A relative minimum can be seen in precipitation over the Maritime Continent (110° E) which is also a feature found in observations based on other variables and data sets which may be attributable to intraseasonal surface flux anomaly contrasts between land and ocean surfaces (see Sobel et al., 2009).

The composite structure of the control simulation (Fig. 3.10, top left) shows a very weak amplitude oscillation with no significant precipitation signal and incoherent propagation. Setting the minimum entrainment parameter to a non-zero value immediately leads to higher amplitude propagating anomalies (Fig. 3.10, top right). Anomalies for the $\alpha = 0.2$ run propagate at 5 m s^{-1} on average, slightly slower than observations. Increasing the minimum entrainment parameter greater than $\alpha = 0.2$ yields zonal wind anomaly propagation speeds comparable to observations, at roughly 7 m s^{-1} (Fig. 3.10, middle row). Zonal wind anomalies are generally stronger than observations as was shown in previous analysis, although precipitation anomalies are of comparable amplitude to observations between 140° E and 180° E. West of this region the amplitude of precipitation anomalies has less agreement with observations, whether they be too strong (120° E - 140° E) or too weak (60° E - 120° E). The weak intraseasonal variability in the Indian Ocean is consistent with previous analysis using related versions of the NCAR CAM (e.g. Maloney and Sobel, 2004).

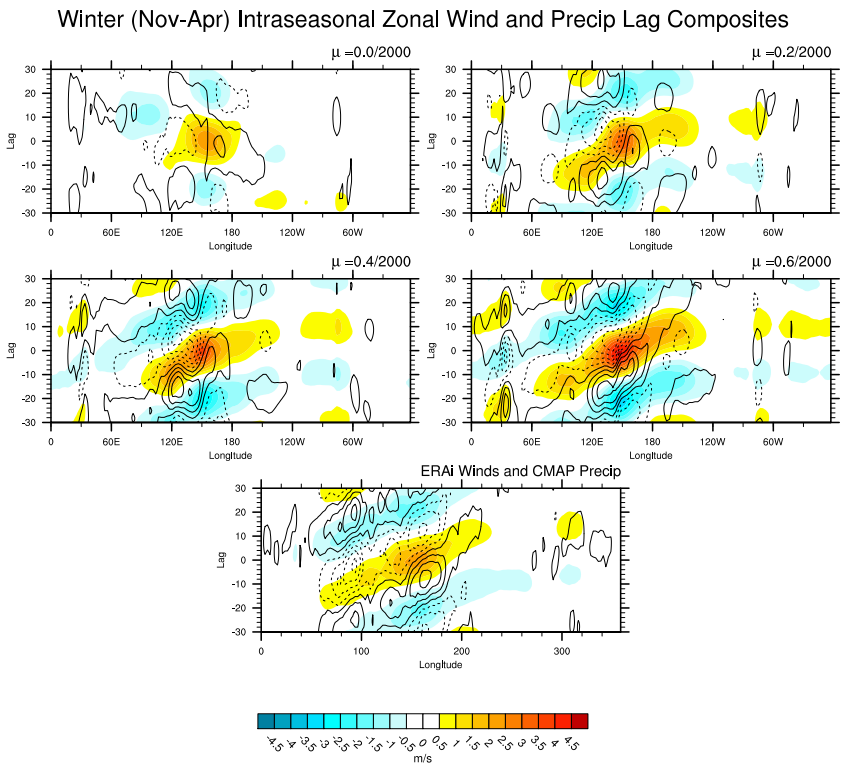

Figure 3.10. Winter (Nov-Apr) 30-90 day filtered 850 hPa zonal wind and precipitation composites as a function of lag based on peak filtered zonal wind. Zonal wind is shown in colors and precipitation in contours with negative values dashed. Data was averaged from 10N – 10S before compositing. Contour interval for precipitation is 0.75 mm day^{-1}.

To examine the vertical structure of ISO events, lag composites were also constructed for specific humidity profiles at 155° E (Fig. 3.11). To construct these composites, filtered data were equatorially averaged from approximately 10 N to 10 S. In all panels of Figure 3.11 the lag in days relative to the peak westerly wind is shown on the abscissa. Since we are considering filtered data whose dominant signal is that of the eastward propagating ISO, the abscissa can also be thought of as an indicator of physical position relative to 155° E. Each day roughly corresponds to six degrees of longitude. The two lower panels show ERA40 and ERAi data. ERA40 was included to show that ERAi is consistent since ERAi has not been used much in the literature at this time, although it should be noted that the ERA40 data used here only considers twelve years of data from 1990-2001. Several previous observational studies have found a westward tilt to specific humidity anomalies as is shown here (e.g. Sperber, 2003; Kiladis et al.,

2005), although this type of composite structure has been shown to vary between the time period and dataset being considered (Kim et al., 2009). Myers and Waliser (2003) noted that the westward tilt commonly associated with profile composites such as these is mostly dominant over the Indian Ocean and transitions to an eastward tilt as it moves from the western Pacific to the central Pacific (see also Tian et al., 2006), however, this is not noticeable in this analysis.

The top left panel of Figure 3.11 shows the lag composite of filtered specific humidity for the control simulation ($\alpha = 0.0$). Although there is a hint of a signal, it is likely an artifact of the compositing technique since the amplitude is so small compared to the other simulations. The top right panel of Figure 3.11 shows the simulation with the smallest non-zero minimum entrainment parameter and we can see that this immediately results in a more appreciable intraseasonal signal, with hints of a westward tilt with height. The magnitude of specific humidity anomalies in the model with the highest minimum entrainment parameter is overestimated compared to observations (Fig. 3.11, middle right). The peak anomalous specific humidity in all model configurations with a non-zero minimum entrainment is much more focused in the middle troposphere than observations which have a broader maximum. This could be due to the minimum entrainment parameter being overly constrictive in such a way that the deep convection anomaly associated with an ISO event becomes unrealistically exaggerated.

A westward tilt with height is apparent in these simulations which is consistent with previous observational results. However, there is less of a westward tilt as the minimum entrainment parameter is increased (Fig. 3.11, middle row). The westward tilt found in other studies has been attributed to low-level moistening, possibly by shallow convection, which has been suggested to be necessary to precondition the atmosphere for the following deep convective phase of the ISO (Benedict and Randall, 2007, 2009; Thayer-Calder and Randall,

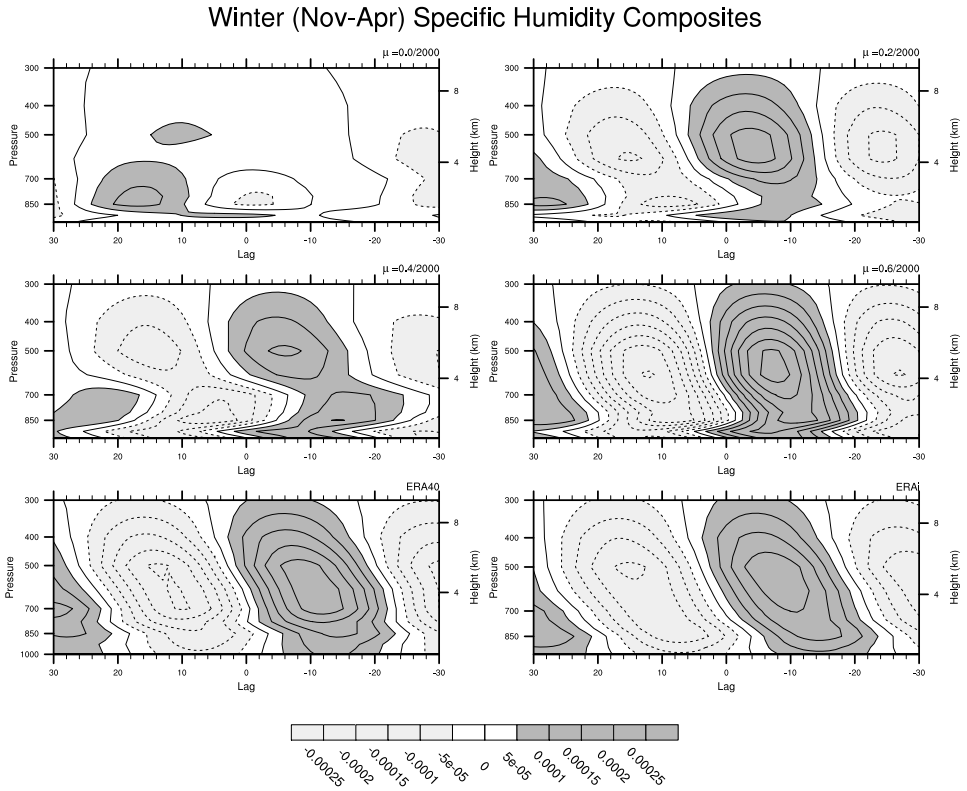

Figure 3.11. Winter (Nov-Apr) 30-90 day filtered specific humidity composites as a function of lag based on peak filtered zonal wind. Data was averaged from 10N – 10S before compositing.

2009). Other studies have suggested that horizontal advection may play a significant role in this moistening ahead of ISO convection. The results presented here seem to suggest that this westward tilt is not a necessary condition for an ISO event since a stronger signal in the model is associated with a decreased westward tilt. In fact, simulations of the ISO in an aqua-planet version of the model shown here are not characterized by a westward tilt with height (Maloney et al., 2009). In their results, the entire column appears to moisten to the east of ISO convection in association with horizontal advection. It appears that the dominant factor which causes the increased intraseasonal signal in the model is the ability to produce strong moisture-convection feedbacks which suppresses convection in regions of dry free tropospheric air and supports robust moisture transports, which is consistent with moisture mode theory.

4. PROCESS ORIENTED DIAGNOSTICS

This section serves to present the results of further diagnostic analysis focused on revealing the key processes leading to enhanced intraseasonal variability in the model when a higher minimum entrainment rate parameter is used. This section discusses the importance of changes to the basic state as well as factors that influence the gross moist stability (GMS) of the tropical atmosphere. Additional model integrations are analyzed which highlight the effect of the rain re-evaporation fraction parameter in enhancing intraseasonal variability. Such analysis provides evidence to strengthen the argument that the simulated ISO is driven by a moisture mode instability supported by strong moisture-convection feedbacks that are enhanced by the inclusion of a non-zero minimum entrainment parameter.

4.1. Mean State

The degree to which the basic state can influence the ISO has been a subject of on ongoing debate. Previous studies have presented contrasting evidence as to whether or not changes to the basic state can significantly influence a model's intraseasonal variability. Analysis of the basic state of the model is presented here to further explore this question.

4.1.1. Moisture and Temperature

Maloney and Hartmann (2001) discussed how convective parameterizations modifications fostered improvements to the simulated intraseasonal variability in an older version of the model used here, with some sensitivity results similar to the results presented in

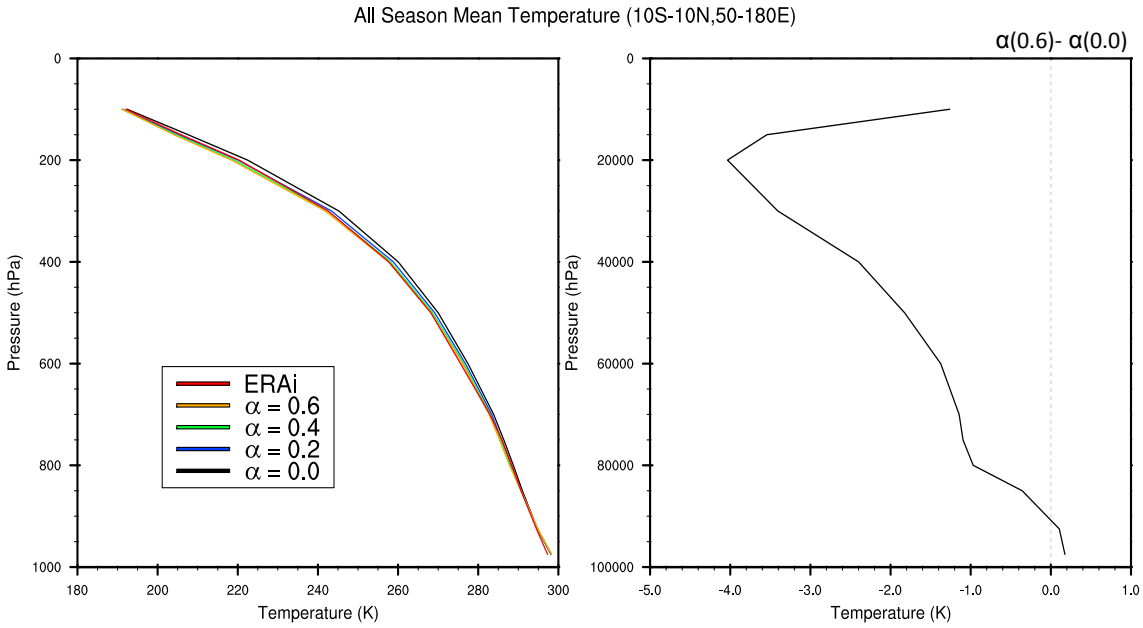

Figure 4.1. All season mean temperature profile for the region 10S – 10 N and 50 E – 180 E (left). The difference between the mean profiles of the runs with the highest (*α=0.6*) and lowest (*α=0.0*) minimum entrainment thresholds is shown in the right panel.

section 3. They added a Tokioka-like trigger based on a critical relative humidity threshold into a version of the Arakawa-Schubert convection scheme and examined the sensitivity of the simulated ISO to variations in rain re-evaporation fraction as well convective downdrafts. Their results show that enhanced intraseasonal variability was accompanied by increased mean-state tropospheric moisture with increased rain re-evaporation and downdraft mass fluxes. They concluded that a more realistic moisture climatology was necessary for accurately reproducing the ISO. Maloney (2009) also reproduced this sensitivity to re-evaporation fraction using the NCAR CAM 3 with a RAS convection scheme implemented. On the other hand, Lin et al. (2008) showed that changing the moisture trigger in a simplified Arakawa-Schubert scheme, as well as other convective parameterizations, in the Seoul National University GCM did not yield a significantly different time-mean simulation of total precipitable water, even though the ISO was consequently enhanced. Hence the precise means by which basic state humidity affects the

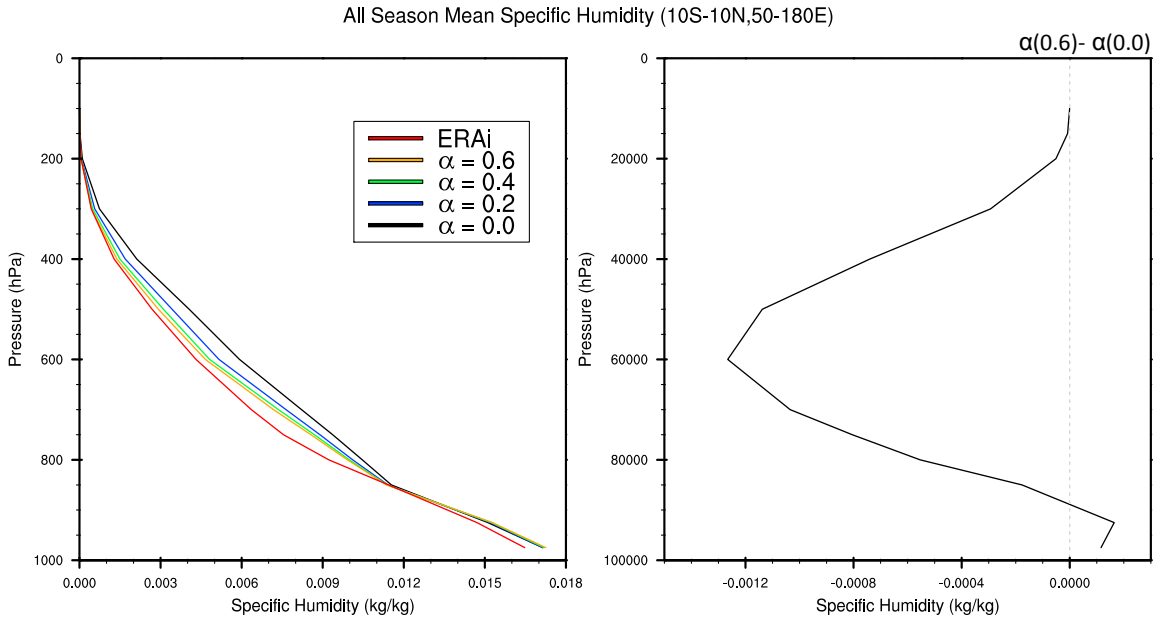

Figure 4.2. All season mean specific humidity profile for the region 10S – 10 N and 50 E – 180 E (left). The difference between the mean profiles of the runs with the highest (*α=0.6*) and lowest (*α=0.0*) minimum entrainment thresholds is shown in the right panel.

simulation of intraseasonal variability is inconsistent among models and hence still a matter of debate.

Figure 4.1 shows the time averaged profile of temperature over the Indo-Pacific region (10N-10S, 50-180E) for all model configurations and ERAi data (left) as well as the difference between the mean profiles. The observed temperature profile (red) is cooler than the control simulation (black) in the middle and upper troposphere. Model runs with non-zero values of the minimum entrainment parameters are generally cooler and lie closer to the observed profile at all levels. The difference between the *α=0.6* and the *α=0.0* runs (Fig. 4.1, right) shows a surprisingly large difference of up to 4 K at upper levels. A cooler profile with a higher minimum entrainment rate is to be expected given that diabatic heating aloft should be reduced as deep convection is suppressed. This explanation would also account for the largest temperature

change occurring at the top of the troposphere since the clouds that reach these levels are suppressed more heavily than those in the middle and lower troposphere.

Figure 4.2 is similar to Figure 4.1, but for specific humidity. A much larger difference exists between model configurations. Excluding the 850 hPa level where all models are in good agreement with observations, all simulations prove to be wetter than ERAi. Below 850 hPa there is no appreciable change in mean specific humidity with increasing minimum entrainment threshold. Above 850 hPa the model shows an interesting response. As the minimum entrainment parameter is ramped up, the amount of moisture in the middle and upper troposphere is significantly decreased. This causes the model's vertical profile to converge to that of ERAi, although it remains too moist. This change was found to be robust for all areas of the Indian and West Pacific oceans. The difference between the $\alpha=0.6$ and the $\alpha=0.0$ runs (Fig. 4.2, right) indicates that the drying is maximized in the middle troposphere, although given that the amount of moisture at the top of the troposphere is so low to begin with, we shouldn't expect the change at upper levels to be as drastic.

This result is the opposite of what was found by Tokioka et al. (1988) in which the column moistened significantly as the threshold of the moisture trigger was increased. One possible reason for this is the effect of the relaxation parameter in RAS which was noted by Chao and Deng (1998) to suppress convection when the relaxation timescale is increased. Another possible reason for the difference in results is that the model used by Tokioka et al. (1988) was an aqua planet with zonally uniform SSTs. Since the model used here has large land masses, this can allow for the advection of dry air into the region of interest. Maloney (2008) showed that intraseasonal variations of horizontal moisture advection were an important aspect of the simulated ISO in a similar configuration of this model, which supports this notion.

Suppression of the deepest clouds through a minimum entrainment threshold both decreases tropospheric humidity and increases intraseasonal variability. As will be shown below, strong mutual interactions between column integrated water vapor and convection occur in the model. Since there is no increase of moisture at lower levels we can conclude that the changes to the convective parameterization does not result in enhanced low-level convective clouds, but rather the clouds that would otherwise form less diluted by environmental air are not allowed to form at all, which appears to dry the troposphere in the model. It appears that further suppression of convective clouds, which influence the moisture in the free troposphere, is needed to have better agreement with ERAi data. The result shown here is interesting in that it contradicts the finding of Maloney and Hartmann (2001) and Maloney (2009) that a moister equatorial troposphere supports increased intraseasonal variability. Thus, there appears to be no unique relationship between mean tropospheric water vapor content and intraseasonal variability.

4.1.2. Diabatic and Radiative Heating

In addition to diagnosing the impact of convective parameterization modifications on the basic state, we can more directly diagnosis how clouds are being suppressed with increased entrainment thresholds by looking at the mean diabatic heating profiles. All-season average diabatic heating profiles are shown for all model runs in Figure 4.3 (left) for the Indo-Pacific region (10N-10S, 50-180E). Comparing the run with the highest minimum entrainment threshold ($\alpha = 0.6$) and the control ($\alpha = 0.0$), a very large difference exists at upper levels centered around 200 hPa, which is statistically significant at the 95% confidence level (Fig. 4.3, right), such that mean upper tropospheric heating is substantially reduced in the $\alpha = 0.6$ case relative to the $\alpha = 0.0$ case. This reduction in heating clearly shows the effect of suppression of deep convective

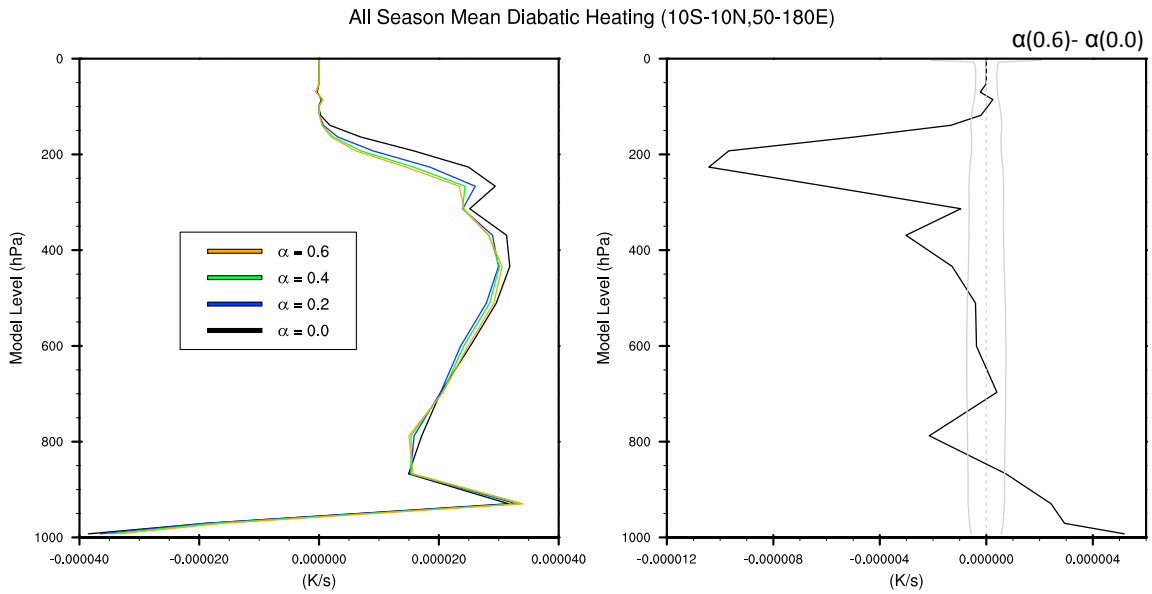

Figure 4.3. All season mean diabatic heating profile (left) and the difference between model runs with α = 0.6 and α = 0.0 (right) for the region 10S – 10 N and 50 E – 180 E. Solid gray lines indicate 95% confidence limits. The dashed gray line indicates a difference of zero.

clouds which detrain at the highest levels of the troposphere. As will be argued below, for an atmosphere with weak temperature gradients in which diabatic heating is nearly balanced by adiabatic cooling associated with ascent, this implies significant changes to upper tropospheric divergence which has significant impacts on the column-integrated moist static energy budget.

The mean radiative heating rate over the Indo-Pacific region (Fig. 4.4, left) shows a larger relative change with increasing minimum entrainment than that of diabatic heating in the lower and middle troposphere. The plot of the difference between the run with the highest minimum entrainment (*α = 0.6*) and the control (*α = 0.0*) shown in Figure 4.4 (right) highlights this adjustment at lower levels but also shows a large statistically significant difference at the top of the troposphere and in the lower stratosphere. The enhanced heating at upper levels is most likely dominated by changes in longwave heating. This combined with the decreased heating at lower levels suggests that the model with *α = 0.6* has a diminished green house effect

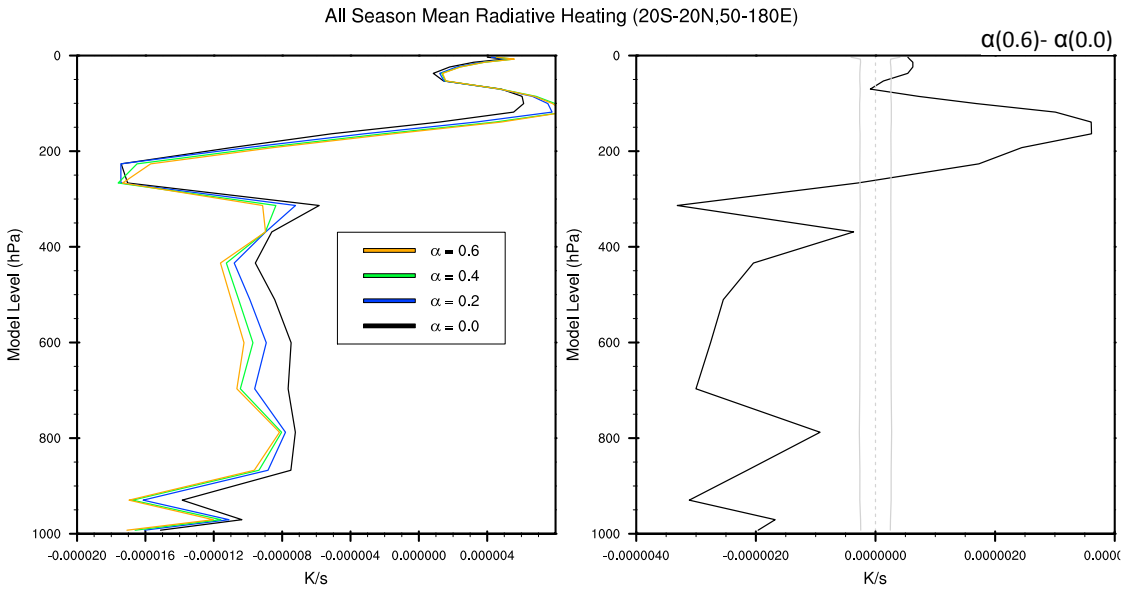

Figure 4.4. All season mean radiative heating profile (left) and the difference between model runs with α = 0.6 and α = 0.0 (right) for the region 10S – 10 N and 50 E – 180 E. Solid gray lines indicate 95% confidence limits. The dashed gray line indicates a difference of zero.

do to the reduction of deep convective towers in the mean and their impact on the longwave energy budget as well as the reduced moisture content of the column.

4.2. The Relationship between Moisture and Precipitation

4.2.1. Moisture-Convection Feedbacks

Several studies have shown that there is a strong relationship between average precipitation and the amount of tropospheric humidity using various sources such as cloud resolving models (Derbyshire et al., 2004; Raymond and Zeng, 2005), satellite observations (Bretherton et al., 2004; Peters and Neelin, 2006), and conventional sounding and radar data (Raymond et al., 2007). These results suggest that sensitivity to free tropospheric humidity can allow dry tropospheric air to inhibit the formation of deep convection. These results are also consistent with the ability for deep convection to moisten the column (i.e. moisture-convection feedbacks). If water vapor anomalies dominate moist static energy anomalies and the gross

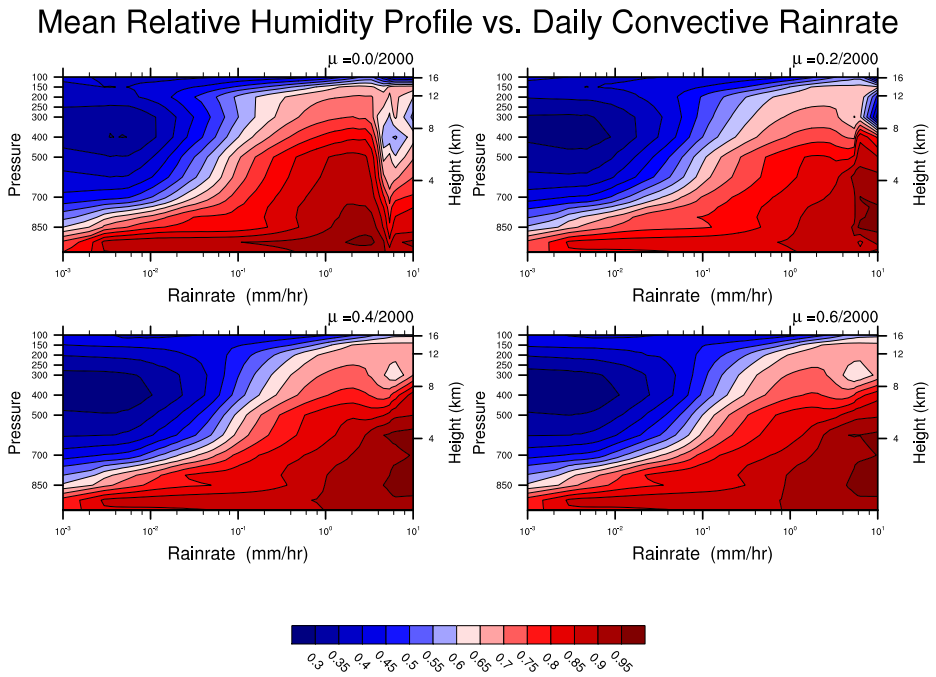

Figure 4.5. Average profile of relative humidity vs. daily average rain rate for all model configurations.

moist stability of the tropical atmosphere is weak or negative, the action of convection can lead to growth of humidity anomalies in the column.

Figure 4.5 shows composite profiles of relative humidity binned as a function of daily convective rain rate from the model. These can be compared to profiles from observations in Thayer-Calder and Randall (2009). The control run (top left) has a dry layer aloft at the highest rain rates (5 - 10 mm hr^{-1}) when compared to profiles associated with lower rain rates (1 - 5 mm hr^{-1}). At lower levels in the control run we see that on average the peak relative humidity does not occur during days with the highest rain rates. This result shows that tropical precipitation in the control model is not strongly related to the level of saturation in the column, unlike the previous observational results discussed above (e.g. Thayer-Calder and Randall, 2009). This result is clearly unrealistic.

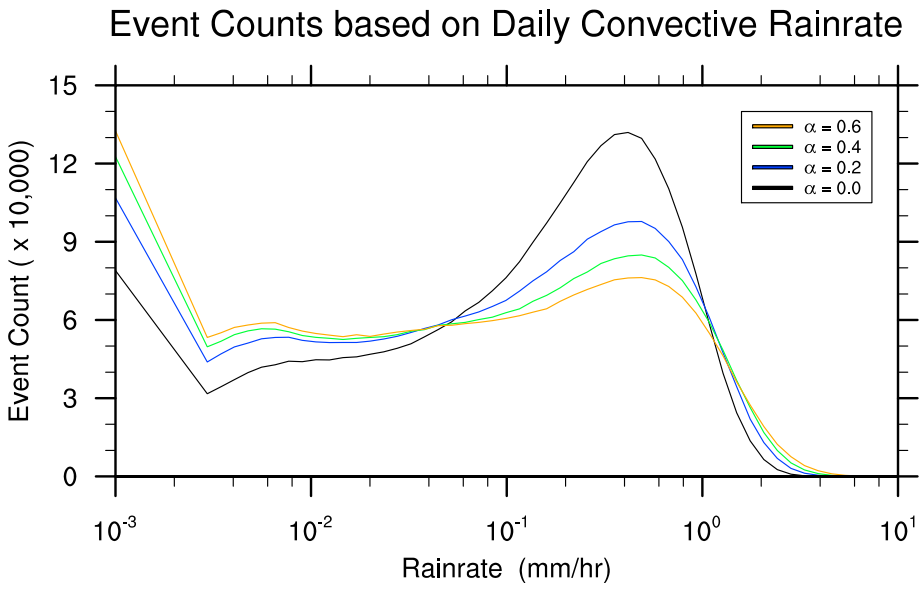

Figure 4.6. Histogram of number of events found for each rain rate bin used to create Figure 4.5.

For the lowest non-zero minimum entrainment parameter ($\alpha = 0.2$) the peak relative humidity occurs only at the highest rain rates (Fig.4.5, top right). Interestingly, there is generally higher relative humidity aloft at high rain rates compared to the control run, but the dry layer mentioned in the previous run appears to be less prominent but still present for the very highest rain rates. This may be a remnant of the deficiency of RAS in the control run in which undiluted ascent of convective plumes is allowed and hence high rain rates can occur even though the free troposphere is anomalously dry. The dry level near 200 hPa at high rain rates is also present in the other model runs but is significantly reduced in amplitude. There appears to be no significant differences between the models with the two highest minimum entrainment values, indicating that the effect of the minimum entrainment threshold begins to saturate. All three models with a non-zero minimum entrainment parameter have a slightly drier boundary layer for all but the smallest rain rates as well as a drier middle troposphere at low rain rates. A histogram of the number of events found for each rain rate bin used in Figure 4.5 is shown in

Figure 4.6. Compared to the control run, all experiment runs with non-zero minimum entrainment thresholds had more occurrences of heavy and light rain, but less moderate rain (0.1 – 1.0 mm hr^{-1}).

A similar analysis was done by Thayer-Calder and Randall (2009) using a comparable version of the NCAR CAM 3 here but with two different methods of representing convection. When using a conventional convective parameterization they found that the model had a dry layer at low levels for high rain rates similar to the one found here at upper levels. Using an embedded cloud resolving model (CRM) in each grid cell to represent sub-grid cloud processes (super-parameterization) they showed that this dry bias was eliminated and the resulting picture looked much closer to observations. The conventional parameterization used in their study has a CAPE based closure scheme which is somewhat insensitive to free tropospheric moisture. The embedded CRM method resolves this issue but also introduces some of its own biases. Recent simulations of the NCAR CAM 3 with convective closures based on diluted CAPE produce much improved interactions between convection and tropospheric humidity (Neale et al., 2008).

Another way to look at how precipitation in the model is related to the amount of moisture in the column is to look at rain rate binned as a function of column saturation fraction which is the calculated as the ratio of the column integrated specific humidity to the column integrated saturation specific humidity. Figure 4.7 shows daily rain rate as a function of saturation fraction for all model runs and observations (top) and the total number of observations for each saturation fraction bin (bottom). SSM/I total column water vapor and ERAi temperature and surface pressure were used to calculate the saturation fraction from observations. It should be noted that the end result of this analysis depends strongly on which observational dataset is used and hence substantial uncertainty exists in the exact form of the

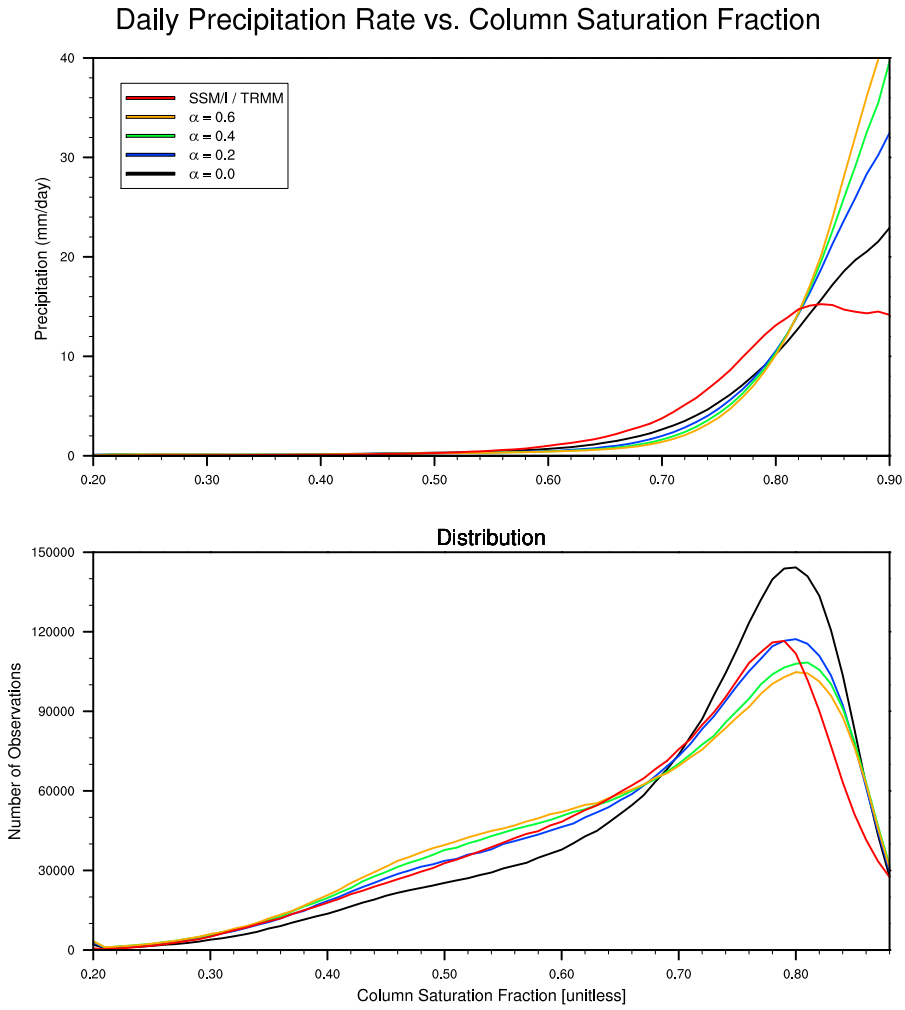

Figure 4.7. Mean daily average precipitation rate (top) and total number of observations (bottom) binned by column saturation fraction for all model runs and observations. Observed data was derived from SSM/I total column water vapor, TRMM precipitation and ERAi temperature and surface pressure for all months in 1998-2001.

observational estimate (see also Bretherton et al., 2004). As the minimum entrainment parameter is increased the dependence of rain rate on saturation fraction becomes progressively more non-linear. This curve also appears to diverge from observations, but given the sensitivity of the observed results to the dataset used in the calculation, confidence in the result is not sufficient to comment on the agreement. Days with moderate levels of saturation fraction (<80%) experience less rain on average given a higher minimum entrainment rate. This is expected given that deep convection should be suppressed for these scenarios. Higher

average rain rates occur for high levels of column saturation fraction, which suggests that the suppression of deep convection leads to more vigorous convection and hence higher rain rates when the column becomes sufficiently close to saturation. The relationship between precipitation and saturation fraction may be too strong in the run with $\alpha = 0.6$ indicating that that the moisture-convection feedbacks are too strong, possibly explaining the overestimated intraseasonal variance discussed previously.

4.2.2 Moist Static Energy Export

Moist static energy (MSE) is a useful quantity for describing the interaction of convection and large-scale circulation since it is approximately conserved for vertical motions in the atmosphere including moist convection. MSE can be defined as

$$m = c_p T + gz + L_v q$$

Where c_p is the specific heat at constant pressure for dry air, T is absolute temperature, g is the gravitational constant, z is height above some reference level, L_v is the latent heat of vaporization, and q is the specific humidity. The first term on the right hand side represents the specific enthalpy, the second term represents potential energy, and the third represents the latent heat content. The direct effect of convection is to vertically rearrange MSE in the atmosphere, but it does not directly affect the vertically integrated MSE. Gross moist stability (GMS) can be defined as the column integrated export of MSE through divergent motions per unit mass flux. This definition can be expanded to account for an effective GMS, which includes the effects of surface fluxes and radiative heating. Lower and upper tropospheric terms which regulate the import and export of MSE into the column mostly cancel each other out, resulting in a small residual. Moisture modes require that the effective GMS be negative (Raymond et al., 2009). This indicates that MSE is being built up in the column in the presence of convection and

the associated divergent motions, which results in convection moistening the environment rather than drying it, as is the case in some models (Raymond and Fuchs, 2009). Gross moist stability can be negative due to the actions of large-scale divergent circulations themselves, or effectively negative if surface fluxes and other MSE sources overcompensate for the loss of MSE by divergent motions.

Yu et al. (1998) estimated small positive values of GMS in regions of the tropics with active convection using prescribed vertical velocity profiles based on quasi-equilibrium assumptions. However, Back and Bretherton (2006) showed that geographic variations in MSE divergence are dominated by differences between the shapes of the vertical motion profiles. Their results found that some areas of the tropics have small values of MSE export with uncertain sign, while the west Pacific warm pool had small positive values. Following the work of Back and Bretherton (2006), MSE export is presented here in light of the issues associated with explicitly calculating GMS.

The calculation of GMS utilizes the terms of the column integrated MSE budget. As in Neelin and Held (1987) and Back and Bretherton (2006), the vertically integrated MSE budget can be written as

$$\left\langle \frac{\partial m}{\partial t} \right\rangle = -\left\langle m \cdot \nabla \mathbf{v} \right\rangle - \left\langle \mathbf{v} \cdot \nabla m \right\rangle + LH + SH + \left\langle LW \right\rangle + \left\langle SW \right\rangle \qquad (4.1)$$

where m is the MSE, LH and SH represent the surface latent and sensible heat flux, and LW and SW represent longwave and shortwave heating rates. Brackets represent a mass-weighted vertical integral from the surface to the top of the troposphere. The pressure is p, ω is the vertical pressure velocity, and **v** is the horizontal wind velocity vector. The gradient operator here only applies along constant pressure surfaces. By using the mass continuity equation in pressure coordinates Raymond and Fuchs (2009) showed that the first term on the right hand

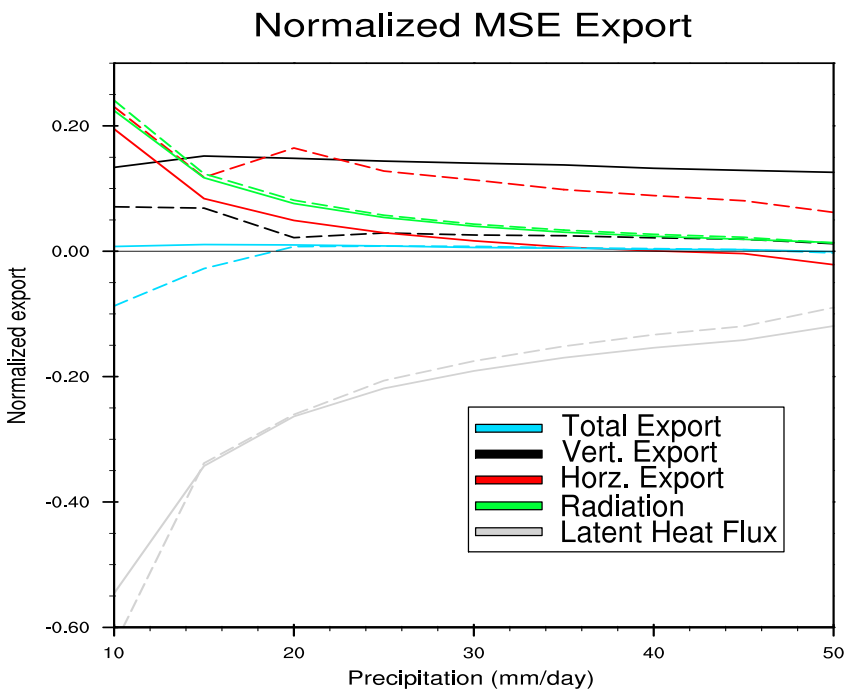

Figure 4.8. Vertically integrated moist static energy budget terms normalized by the dry static energy export as a function of precipitation for runs α = 0.0 (solid) and α = 0.6 (dashed) for the region 18 S – 18 N and 48 – 180 E.

side of Equation 4.1 represents the vertical integral of vertical advection of MSE. We consider this quantity useful here since we are focused on changes to the divergent motions brought about by convection. All terms will be normalized by the column integrated dry static energy export due to divergent motions in order to give dimensionless quantities which are relevant to theories of precipitation.

Figure 4.8 shows the average column integrated MSE budget terms normalized by the dry static energy export for the model runs with $\alpha = 0.0$ (solid line) and $\alpha = 0.6$ (dashed line) as a function of daily rain rate. The export due to vertical motions is shown in black, the export due to horizontal motions in red, the sum of longwave and shortwave heating effects in green, the combined surface latent and sensible heat fluxes in gray, and the total MSE tendency in blue.

The control run shows MSE export by vertical motions being comparable to latent heat flux for rain rates above 40 mm day^{-1}. The uncertainty in values for rain rates lower than 10 mm

day^{-1} is too large to draw any definite conclusions. The change to the radiative component of the MSE budget is miniscule. Changes to the terms which describe the surface fluxes are also small but are likely important to the ISO, especially at low rain rates where the import (i.e. negative export) of MSE in the column is increased in the $\alpha = 0.6$ case, which likely assists in the buildup of column moisture anomalies. The model run with $\alpha = 0.6$ shows a large reduction in MSE export by vertical motions for all rain rates. The horizontal export changes in the opposite sense so that the $\alpha = 0.6$ case has increased the export due to horizontal motions, mostly at moderate to high rain rates. This change likely reflects the role that moisture advection plays in regulating the propagation of the ISO, both by advecting moisture anomalies eastward as well as damping out moisture anomalies by mixing drier air in from higher latitudes (see also Maloney et al., 2009).

The total MSE export is slightly positive for rain rates between 10 and 50 mm day^{-1} in the control run. This illustrates the inability of the control run to sustain moisture anomalies. The $\alpha = 0.6$ run, on the other hand, shows a negative MSE export (i.e. positive MSE import) for low rain rates. This scenario represents a negative effective GMS since the MSE source outweighs the effect of the MSE export. Since moisture convection feedbacks are also enhanced in the $\alpha = 0.6$ case, we can interpret the daily averaged rain rate as analogous to the amplitude of the moisture anomaly in the column. When the column is anomalously dry, and hence the rain rate anomalously low, we find that the column is being moistened by convection and related processes. Then when the column becomes anomalously moist, the MSE export becomes positive and the moisture anomaly (and subsequently convection) is reduced through various processes including horizontal advection. Thus, the timescale of this oscillatory behavior may be determined by the relationship of GMS and precipitation. This provides strong evidence that the Tokioka moisture trigger allows the model to sustain moisture modes.

Figure 4.3 showed a diminished vertical heating profile at upper levels for higher minimum entrainment rates. For a given MSE profile, and approximate correspondence between the profile of diabatic heating and vertical motion, a reduction in upper tropospheric divergence would tend to reduce the effective GMS. Sensitivity analysis suggests that the change in MSE export is dominated by changes to the divergence profile, rather than changes to the MSE profile. Interestingly, changes to the mean divergence profiles as the minimum entrainment is increased are more subtle than those suggested by the diabatic heating profiles and vary in sign throughout the troposphere. An explanation of why this causes the largest change to the MSE export is difficult, since slight changes o the divergence profile appear to generate large changes to the MSE export by divergent motions

4.3. Rain Re-Evaporation Fraction

Maloney and Hartmann (2001) investigated the sensitivity of the simulated ISO to a rain re-evaporation fraction parameter in the community climate system model 3 (CCSM; Kiehl et al., 1998) with the microphysics of cloud with relaxed Arakawa-Schubert (McRAS) parameterization of Sud and Walker (1999). They demonstrated that increasing the rain re-evaporation fraction ϵ lead to an enhanced ISO signal in the model. Using various values of ϵ we can get an idea for how this parameter affects the simulations presented here.

Figure 4.9 shows space time spectra for winter 850 hPa zonal wind for five model configurations arranged so that reading from left to right represents increasing α with fixed ϵ while reading from bottom to top represents increasing ϵ with fixed α. In agreement with Maloney and Hartmann (2001) and Maloney (2009), increasing ϵ produces a larger ISO signal as evidenced by the increased spectral power for thirty to ninety day periods and wavenumbers one through three. The change in intraseasonal variance produced by increasing the minimum

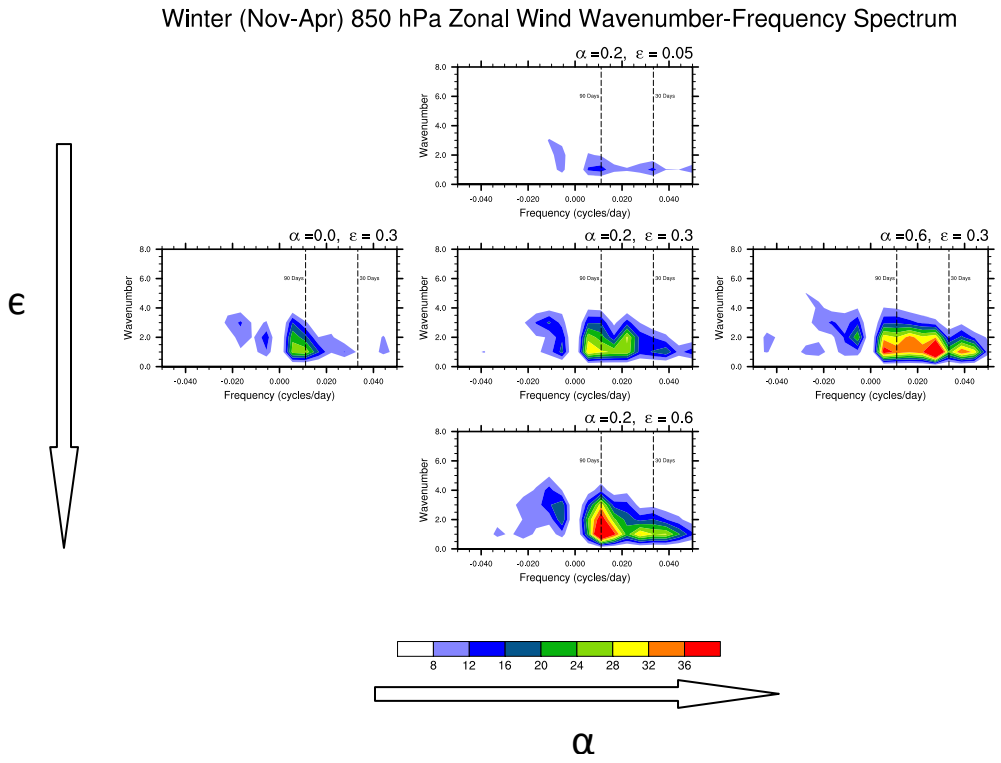

Figure 4.9. Winter (Nov-Apr) 850 hPa zonal wind wavenumber-frequency spectra for model runs with ϵ = 0.3 fixed and α = 0.0 (left), 0.2 (center), 0.6 (right) and model runs with α = 0.2 fixed and ϵ = 0.05 (top), 0.3 (center), and 0.6 (bottom). Spectra were calculated from equatorially averaged data from approximately 10S – 10N.

entrainment produces more power at higher frequencies than that produced by increasing the rain re-evaporation fraction. The spectrum for the highest rain re-evaporation fraction has a large spectral peak at ninety day periods, whereas the largest spectral peak for the highest minimum entrainment occurs closer to 30 days.

Composite lagged specific humidity profiles are shown for boreal winter in Figure 4.10 with a similar layout to Figure 4.9 with increasing α and fixed ϵ shown from left to right and increasing ϵ and fixed α shown from top to bottom. An increased rain re-evaporation fraction results in an appreciable enhancement of the ISO signal in the model. Unlike the effect of increasing the minimum entrainment rate shown in Figure 3.11 in which the westward tilt with height was slightly reduced, the composites shown here indicate that the westward tilt is

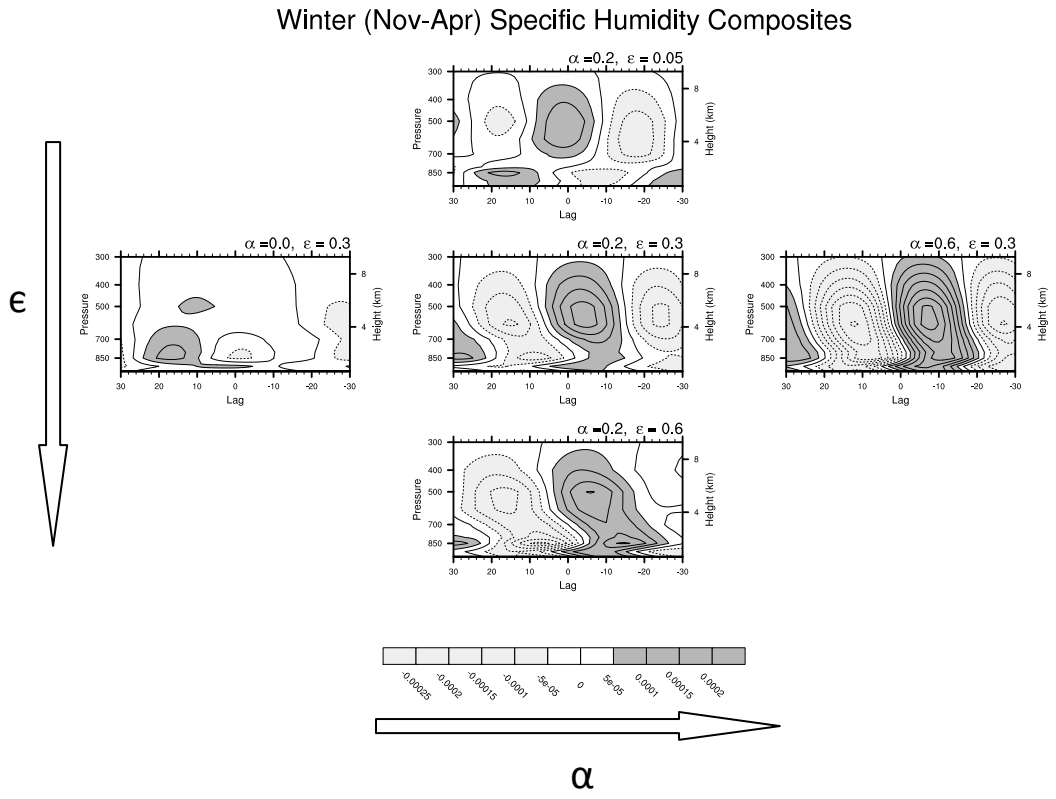

Figure 4.10. Winter (Nov-Apr) lagged specific humidity composites for model runs with ϵ = 0.3 fixed and α = 0.0 (left), 0.2 (center), 0.6 (right) and model runs with α = 0.2 fixed and ϵ = 0.05 (top), 0.3 (center), and 0.6 (bottom). Spectra were calculated from equatorially averaged data from approximately 10S – 10N.

augmented for higher ϵ. This could be because low-level moistening as described by discharge-recharge theories (e.g. Bladé and Hartmann, 1993) plays a more significant role in this configuration than the cloud suppression effects of a non-zero minimum entrainment rate. Maloney (2009) showed that the meridional humidity gradient increases with rain re-evaporation fraction. Low-level advection across this humidity gradient appeared to be responsible for low-level preconditioning as well as the tilted moisture structure in Maloney (2009), and hence may explain the behavior of the model with increasing rain re-evaporation fraction shown here.

Figure 4.11 shows the difference in mean all-season vertical profiles of specific humidity and temperature between the model runs with the highest and lowest minimum entrainment thresholds (solid lines) and between the model runs with the highest and lowest rain re-evaporation fractions (dashed lines). A higher minimum entrainment results in drier and colder conditions on average above the boundary layer, consistent with Figures 4.1 and 4.2. The largest differences are seen in the middle troposphere for specific humidity but near the top of the troposphere for temperature. Increasing the rain re-evaporation fraction produces a moister middle troposphere and a warmer upper troposphere. The low-level temperature response shifts in the opposite sense to that of the upper troposphere, which may be due to enhanced evaporative cooling in the lower troposphere.

The difference between the highest and lowest minimum entrainment runs may be explained by the suppression of deep convection which diminishes the diabatic heating associated with deep convection and moistening due to detrainment. The effect of this change on the GMS might be to decrease the MSE being exported out of the column since there is less MSE in the column overall. Cooler temperatures aloft may also contribute to the less GMS by decreasing the dry static energy export.

The dashed curves suggest that the effect of increased rain re-evaporation fraction may be to enhance mid-level convection, but more analysis is needed to determine what effects are dominant in causing the difference. Stronger re-evaporation possibly causes the column to maintain anomalously moist conditions and sustain deep convective episodes, although causality is difficult to diagnose. Depending on the timescale required to damp out moisture anomalies, this should consequently increase the variance. The moistening of the lower troposphere which results from increasing the rain re-evaporation fraction should increase the gross moisture stratification, which for a given dry static stability, would decrease the GMS.

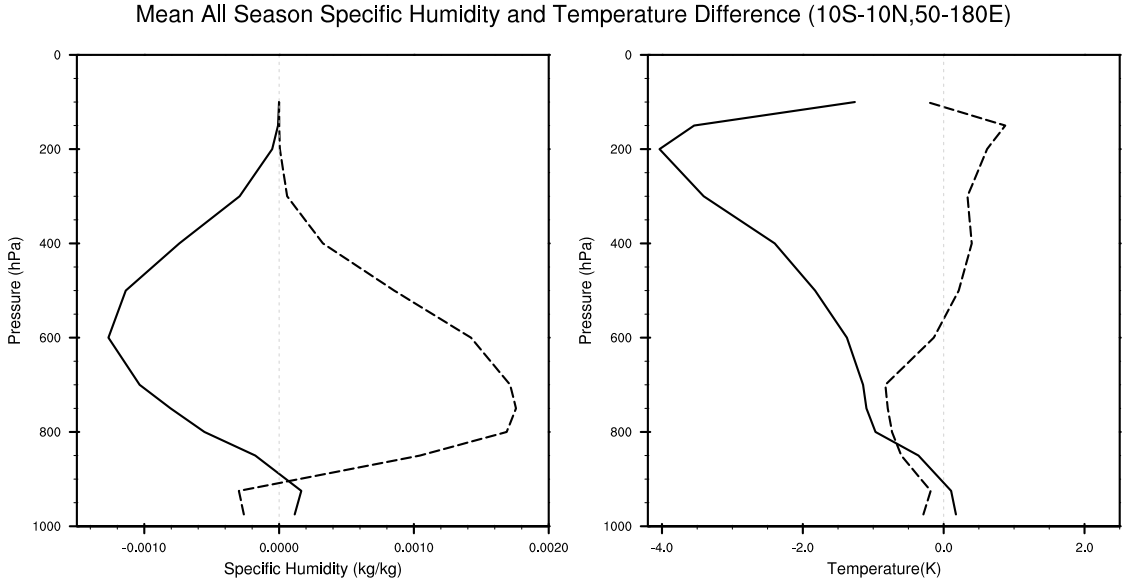

Figure 4.11. All season mean specific humidity (left) and temperature (right) difference between the model run with $\alpha = 0.6$ and $\alpha = 0.0$ (solid) and $\epsilon = 0.6$ and $\epsilon = 0.05$ (dashed). Profiles were calculated over the region 10S – 10 N and 50 E – 180 E.

Given that GMS is a diagnostic quantity which when negative indicates that convection is moistening the column rather than drying it, we should expect that similar analysis as shown in Figure 4.8 of the MSE budget between the model runs with the highest and lowest rain re-evaporation fractions should show a similar decrease in the MSE export by divergent motions.

It is interesting that no straightforward dependence of intraseasonal variability on mean tropospheric humidity is found in the analysis of Figure 4.11. Although both methods increase the intraseasonal variance in the model, increasing the threshold of the Tokioka moisture trigger dries the middle troposphere whereas increasing rain re-evaporation moistens the middle troposphere and increases tropospheric humidity overall. This would seem to belie a simple dependence of the humidity climatology and variability, contrary to that suggested by Maloney and Hartmann (2001).

5. SUMMARY AND DISCUSSION

This study investigated the sensitivity of a simulated intraseasonal oscillation (ISO) to a minimum entrainment rate parameter (see Tokioka et al., 1988) in the NCAR Community Atmosphere Model (CAM) 3.1 with the relaxed Arakawa-Schubert (RAS) convective parameterization. Four sixteen year integrations with minimum entrainment parameters α = *0.0*, *0.2*, *0.4* and *0.6* were analyzed. In section 3 a higher minimum entrainment threshold was shown to produce a more robust ISO in the model. A stronger ISO signal was accompanied by overestimated intraseasonal variance for wind and precipitation when compared to ECMWF interim reanalysis (ERAi) and the Tropical Rainfall Measuring Mission (TRMM) data. Column integrated saturation fraction variance was shown to increase with increased minimum entrainment rate in a manner which converged toward observations in the Indo-Pacific region where the ISO is active. Wind and precipitation composites were presented which highlighted improvements to the horizontal structure and propagation of the ISO with increased minimum entrainment rate (e.g. Fig. 3.10).

Changes to the basic state were also shown to result from increasing the minimum entrainment parameter. Changes to the amplitude and spatial structure of the mean winds and precipitation were found to be similar to previous studies such as Wang and Schlesinger (1999) and Lin et al. (2008) in the sense that the model's basic state became less realistic. For example, Figure 3.1 showed that the winds in the Indian Ocean become stronger easterlies with an increased moisture trigger threshold. These previous studies found that the moisture trigger they employed resulted in slightly diminished precipitation and increased overall zonal wind

speed in the mean. Although these changes to the mean low-level winds and precipitation were small, profiles of average temperature and specific humidity over the Indo-Pacific region showed more noteworthy differences. A cooler and drier atmosphere resulted from the suppression of deep convection by the added Tokioka moisture trigger. Diabatic heating showed a large reduction at upper levels with increasing minimum entrainment threshold, an effect which appeared to saturate for higher thresholds. Increased minimum entrainment rate causes precipitation to have an increasingly non-linear relationship to the amount of moisture in the column. Composite profiles of relative humidity reveal a dry upper troposphere for high rain rates in the control run with no minimum entrainment threshold, which disagrees with observations (see Thayer-Calder and Randall, 2009). Increasing the minimum entrainment parameter was shown to diminish this bias in the model.

In addition to including the modifications used by Tokioka et al. (1988), the model presented also includes another parameter which specifies the rain re-evaporation fraction. Increasing the value of this parameter was shown by Maloney and Hartmann (2001) to augment the ISO signal in a GCM, an effect which was attributed to a moister mean troposphere. Increasing the rain re-evaporation in the model presented here produced similar results. The ISO produced from using a high rain re-evaporation fraction and moderate minimum entrainment showed spectral power to be concentrated at the lowest frequencies of the intraseasonal band (30-90 days) and had a sharper westward tilt with height when compared to the model run with a high minimum entrainment rate and moderate rain re-evaporation fraction. Interestingly, increasing the minimum entrainment threshold dries the troposphere in the mean, whereas increasing rain re-evaporation fraction moistens it. The fact that implementation of both parameters support more robust intraseasonal variability suggests no straight forward

correspondence exists between intraseasonal humidity and the basic state humidity, in contrast to the conclusions of Maloney and Hartmann (2001) and Maloney (2009).

Results presented here suggest that the ISO which is enhanced through a Tokioka moisture trigger resembles that of a moisture mode (see also Maloney et al., 2009), in which the location of convection is regulated by the processes controlling tropospheric humidity. Intraseasonal saturation fraction variance (Fig. 3.3) shows that the control run lacks substantial variance of column moisture content in the Indo-Pacific region while the $\alpha = 0.6$ run shows increased variance in this area. This result, along with the increasingly non-linear dependence of rain rate on column saturation fraction, suggests that the minimum entrainment parameter allows the model to support robust moisture-convection feedbacks by modifying the convective parameterization to be more responsive to the amount of moisture in the free troposphere. Convection under a higher minimum entrainment threshold appears to be less effective at discharging moisture from the column, and through the added contributions of surface latent heat fluxes, lead to growth of moisture anomalies. In other ISO studies which highlight the role of a localized discharge-recharge cycle, a westward tilt with height to humidity anomalies was attributed vertical moistening, possibly by shallow convection (e.g. Kiladis et al., 2005; Agudelo et al., 2006). A diminished westward tilt with height is shown in the time vs. height composite structure of specific humidity anomalies as the minimum entrainment rate is increased (Fig. 3.11). This suggests that the low-level moistening ahead of deep convection associated with the ISO may not be a necessary feature for producing strong variability in the model. This has also been suggested by other recent studies such as Maloney (2009) and Maloney et al. (2009). In these studies, the westward tilt with height was associated with horizontal moisture advection.

Moisture modes are identical to the class of tropical large-scale modes which were demonstrated by Sobel et al. (2001) to exist under the weak temperature gradient (WTG)

approximation. For a moisture mode to be excited, negative effective gross moist stability (GMS, see Raymond et al., 2009), which includes the effects of surface fluxes and radiative heating as MSE sources, must be achieved (Raymond and Fuchs, 2009). The suppression of deep convection with the Tokioka moisture trigger acts to reduce the mean export of MSE out of the column which becomes negative for low rain rates (Fig. 4.8). This is likely because of changes to the profile of divergence with increasing minimum entrainment rate. These results agree with the suggestion of Raymond and Fuchs (2009) that effective GMS is a good diagnostic quantity for investigating a model's ability to produce a robust ISO.

Alternative methods of representing the effects of convection in GCMs by embedding cloud resolving models into each grid cell known as a multiscale modeling framework (i.e. super-parameterization; e.g. Khairoutdinov et al., 2008) have been shown to improve many aspects a model's variability (e.g. Thayer-Calder and Randall, 2009; Benedict and Randall, 2009). When using such methods, convection more naturally interacts with environmental moisture. Making use of these methods to investigate processes such as moisture-convection feedbacks in finer detail will most definitely prove to be beneficial.

There are likely other processes which contribute to producing an ISO in this model. The role of shallow convective moistening at low-levels to the east of the deep convection associated with the ISO did not appear to be a significant factor when the Tokioka moisture trigger threshold was increased. Analysis of the role of shallow convection in the MSE budget in a super-parameterized model may illuminate whether this process contributes to the dynamics of the ISO. The role of WISHE was not investigated here, but various other studies have shown the importance of this process in producing an ISO in a GCM. A realistic representation of wind induced surface latent heat flux anomalies (Maloney and Sobel, 2004) in addition to accurate basic state westerlies (Inness et al., 2003) can significantly impact the intraseasonal variability of

a GCM. This importance of basic state westerlies is supported in the recent analysis of aquaplanet simulations with varying basic state sea surface temperature distributions in Maloney et al. (2009). It is interesting to note that the mean-state westerlies at 850 hPa over the Indian Ocean tend to decrease and become easterly with increased minimum entrainment rate while the mean westerly winds over the maritime continent become slightly stronger. Given the notion that the eastward propagation of a moisture mode is mostly driven by the horizontal advection of the mean westerly winds, it would seem that this should diminish the ISO signal over the Indian Ocean, which is not evident in the results. The increased spectral power at higher intraseasonal frequencies as well as the difference in propagation speed between the $\alpha = 0.4$ and $\alpha = 0.6$ simulations may be partially explained by the change in the mean winds.

Plans for future work include performing similar analysis on a multiscale modeling framework such as the NCAR super-parameterized CAM. Further modeling efforts to determine the extent to which horizontal advection drives the eastward propagation of the ISO will be useful in determining the degree to which moisture mode theory applies to the dynamics of the ISO. This includes mechanism denial experiments in which horizontal moisture advection is held to a fixed climatological value. It may also be interesting to look at this with respect to the meridional excursions exhibited by the observed ISO. Observational evidence for the slowing of the ISO with weakening of the basic state westerlies in the Indian and Pacific Oceans may also support this hypothesis.

REFERENCES

1. Agudelo, P. A., J. A. Curry, C. D. Hoyos, and P. J. Webster, 2006: Transition between suppressed and active phases of the intraseasonal oscillations in the Indo-Pacific warm pool. *J. Climate*, 19¸ 5519-5530.

2. Arakawa, A., and W. H. Schubert, 1974: Interaction of a cumulus cloud ensemble with the large-scale environment, Part I. *J. Atmos. Sci*., 31, 647-701.

3. Araligidad, N. M., and E. D. Maloney, 2008: Wind driven latent heat flux and the intraseasonal oscillation. *Geophy. Res. Lett*., 35, L04815, doi:10.1029/2007GL032746.

4. Back, L. E., and C. S. Bretherton, 2006: Geographic variability in the export of moist static energy and vertical motion profiles in the tropical Pacific. *Geophsy. Res. Lett*., 33, L17810, doi: 10.1029/2006GL026672.

5. Benedict, J. J., and D. A. Randall, 2007: Observed characteristics of the MJO relative to maximum rainfall. *J. Atmos. Sci.*, 64, 2332-2354.

6. Benedict, J. J., and D. A. Randall, 2009: Structure of the Madden-Julian Oscillation in the Superparameterized CAM. *J. Atmo. Sci*., in press.

7. Bergman, J. W., H. H. Hendon, and K. M. Weickmann, 2001: Intraseasonal air-sea interactions at the onset of El Niño. *J. Climate*, 14, 1702-1719.

8. Bladé, I. and D. L. Hartmann, 1993: Tropical intraseasonal oscillations in a simple nonlinear model. *J. Atmos. Sci*., 50, 2922-2762.

9. Bretherton, C. S., M. E. Peters, and L. E. Back, 2004: Relationships between water vapor path and precipitation over the tropical oceans. *J. Climate*, 17, 1517-1528.

10. Camargo, S. J., M. C. Wheeler, and A. H. Sobel, 2009: Diagnosis of the MJO modulation of tropical cyclogenesis using an empirical index. *J. Atmos. Sci.*, early online, doi:10.1175/2009JAS3101.1.

11. Chang, C. P., 1977: Vicious internal gravity waves and low-frequency oscillations in the tropics, *J. Atmos. Sci*., 34, 901-910.

12. Chao, W. C., 1995: A critique of wave-CISK as an explanation for the 40-50 day tropical intraseasonal oscillation. *J. Meteor. Soc. Japan*, 73, 677-684.

13. Chao, W. C., and S-J. Lin, 1994: Tropical intraseasonal oscillation, super cloud clusters, and cumulus convection schemes. *J. Atmos. Sci.,* 51, 1282-1297.

14. Chao, W. C., and L. Deng, 1998: Tropical intraseasonal oscillation, super cloud clusters, and cumulus convection schemes. Part II: 3D aqua-planet simulations. *J. Atmos. Sci.,* 55, 690-709.

15. Cho, H.-R. and D. Pendlebury, 1997: Wave-CISK of equatorial waves and the vertical distribution of cumulus heating. *J. Atmos. Sci.*, 54, 2429-2440.

16. Collins, W. D., and Coauthors, 2006: The formulation and simulation of the Community Atmosphere Model: CAM3. *J. Climate*, 19, 2144-2161.

17. Derbyshire, S. H., I. Beau, P. Bechtold, J.-Y. Grandpeix, J.-M. Piriou, J.-L. Redelsperger, and P. M. M. Soares, 2004: Sensitivity of moist convection to environmental humidity. *Quart. J. Roy. Meteor. Soc.*, 130, 3055-3079.

18. Duffy, P. B., B. Govindasamy, J. P. Iorio, J. Milovich, K. R. Sperber, K. E. Taylor, M. F. Wehner, and S. L. Thompson, 2003: High-resolution simulation of global climate, part I: Present climate. *Climate Dyn.*, 21, 371-390.

19. Emanuel, K. A., 1987: Air-sea interaction model of intraseasonal oscillations in the Tropics. *J. Atmos. Sci.*, 44, 2324-2340.

20. Emanuel, K. A., 1993: The effect of convective response time on WISHE modes. *J. Atmos. Sci.*, 50, 1763-1775.

21. Fuchs, Z., and D. J. Raymond, 2007: A simple, vertically resolved model of tropical disturbances with a humidity closure. *Tellus*, 59A, 344-354.

22. Gill, A. E., 1980: Some simple solutions for heat induced tropical circulation. *Quart. J. Roy. Meteor. Soc.*, 106, 447-462.

23. Hack, J. J., 1994: Parameterization of moist convection in the National Center For Atmospheric Research community climate model (CCM2). *J. Geophys. Res.,* 99, 5551-5568.

24. Hayashi, Y., 1970: A theory of large-scale equatorial waves generated by condensation heat and accelerating the zonal wind. *J. Meteor. Soc. Japan*, 48, 140-160.

25. Hayashi, Y., and A. Sumi, 1986: The 30-40 day oscillations simulated in an “aqua-planet” model. *J. Meteor. Soc. Japan*, 64, 451-467.

26. Hendon, H. H. and M. L. Salby, 1994: The life cycle of the Madden-Julian Oscillation. *J. Atmos. Sci.*, 51, 2225-2237.

27. Higgins, R. W., and K. C. Mo, 1997: Persistent north Pacific circulation anomalies and the tropical intraseasonal oscillation. *J. Climate*, 10, 223-244.

28. Higgins, R. W., J.-K. E. Schemm, W. Shi, and A. Leetmaa, 2000: Extreme precipitation events in the western United States related to tropical forcing. *J. Climate*, 13, 793-820.

29. Houze, R. A., Jr., 1997: Stratiform precipitation in regions of convection: A meteorological paradox? *Bull. Amer. Meteor. Soc.*, 78, 2179-2196.

30. Hu, Q., and D. Randall, 1994: Low frequency oscillations in radiative-convective systems. *J. Atmos. Sci.*, 51, 1089-1099.

31. Hung, C.-W. and M. Yanai, 2004: Factors contributing to the onset of the Austrailian summer monsoon. *Quart. J. Roy. Meteor. Soc.*, 130, 739-758.

32. Inness, P. M., J. M. Slingo, S. J. Woolnough, R. B. Neale, and V. D. Pope, 2001: Organization of tropical convection in a GCM with varying vertical resolution: Implications for the simulation of the Madden-Julian Oscillation. *Climate Dyn.*, 17, 777-793.

33. Inness, P. M., J. M. Slingo, E. Guilyardi, and J. Cole, 2003: Simulation of the Madden-Julian Oscillation in a coupled general circulation model II: The role of the basic state. *J. Climate*, 16, 365-282.

34. Itoh, H., 1989: The mechanism for the scale selection of tropical intraseasonal oscillations. Part I: Selection of wavenumber 1 and the three-scale structure. *J. Atmos. Sci.,* 16, 1779-1798.

35. Jones, C. and B. C. Weare, 1996: The role of low-level moisture convergence and ocean latent heat fluxes in the Madden-Julian Oscillation. *J. Climate*, 9, 3086-3104.

36. Kemball-Cook, S. R. and B. C. Weare, 2001: The onset of convection in the Madden-Julian Oscillation. *J. Climate*, 14, 780-793.

37. Khairoutdinov, M., C. DeMott and D. Randall, 2008: Evaluation of the simulated interannual and subseasonal variability in an AMIP-style simulation using the CSU Multi-scale Modeling Framework. *J. Climate.* 21, 413-431.

38. Kiehl, J. T., J. J. Hack, G. B. Bonan, B. A. Boville, D. L. Williamson, and P. J. Rasch, 1998: The national center for atmospheric research community climate model: CCSM3. *J. Climate*, 11, 1131-1150.

39. Kiladis, G. N., K. H. Straub, and P. T. Haertel, 2005: Zonal and vertical structure of the Madden-Julian Oscillation. *J. Atmos. Sci.*, 62, 2790-2809.

40. Kim, D. and Coauthors, 2009: Application of MJO simulation diagnostics to climate models. *J. Climate*, in press.

41. Kuma, K.-I., 1994: The Madden-Julian Oscillation and tropical disturbances in an aqua-planet version of JMA global model with T63 and T159 resolution. *J. Meteor. Soc. Japan*, 72, 147-172.

42. Kuo, Y. H., 1974: Further studies of the parameterization of the influence of cumulus convection of large-scale flow. *J. Atmos. Sci.,* 31, 1232-1240.

43. Lau, K.-M., and P. H. Chan, 1986: The 40-50 day oscillation and the El Niño/ Southern Oscillation – A new perspective. *Bull. Amer. Meteor. Soc.*, 67, 533-534.

44. Lau, K.-M., and T. J. Phillips, 1986: Coherent fluctuations of extratropical geopotential height and tropical convection in intraseasonal time scales. *J. Atmos. Sci.*, 43,1164-1181.

45. Lau, N.-C., and K.-M. Lau, 1986: Structure and propagation of intraseasonal oscillations appearing in a GFDL GCM. *J. Atmos. Sci.*, 43, 2023-2047.

46. Lawrence, D. M., and P. J. Webster, 2002: The boreal summer intraseasonal oscillation: relationship between northward and eastward movement of convection, *J. Atmos. Sci.*, 59, 1593-1606.

47. Lee, M.-I., I.-S. Kang, and B. E. Mapes, 2003: Impacts of cumulus convection parameterizations on aqua-planet AGCM simulations of tropical intraseasonal variability. *J. Meteor. Soc. Japan,* 81, 963-992.

48. Liebmann, B., H. Hendon, and J. Glick, 1994: The relationship between tropical cyclones of the western Pacific and Indian oceans and the Madden-Julian Oscillation. *J. Meteor. Soc. Japan*, 72, 401-412.

49. Lim, H., T. K. Lim and C.-P Chang, 1990: Reexamination of wave-CISK theory: Existence and properties of non-linear wave-CISK modes. *J. Atmos. Sci.*, 47, 3078-3091.

50. Lin, J-L., M-I. Lee, D. Kim, I-S Kang and D. M. W. Frierson, 2008: The impacts of convective parameterization and moisture triggering on AGCM-simulated convectively coupled equatorial waves. *J. Climate,* 21, 883-909.

51. Lin, J-L., B. Mapes, M. Zhang, and M. Newman, 2004: Stratiform precipitation, vertical heating profiles, and the Madden-Julian Oscillation. *J. Atmos. Sci.*, 61, 296-309.

52. Lin, J-L., and B. Mapes, 2004: Radiation budget of the tropical intraseasonal oscillation. *J. Atmos. Sci.*, 61, 2050-2062.

53. Lin, J. W.-B., J. Neelin, and N. Zeng, 2000: Maintenance of tropical intraseasonal variability: Impact of evaporation-wind feedback and midlatitude storms. *J. Atmos. Sci.*, 57, 2793-2823.

54. Lin, X. and R. H. Johnson, 1996: Kinematic and thermodynamic characteristics of the flow over the western Pacific warm pool during TOGA-COARE. *J. Atmos. Sci.*, 53, 695-715.

55. Lindzen, R. S., 1974: Wave-CISK in the Tropics. *J. Atmos. Sci.*, 31, 156-179.

56. Lorenz, D. J., and D. L. Hartmann, 2002: The effect of the MJO on the North American monsoon. *J. Climate*, 19, 333-343.

57. Madden, R. A., 1986: Seasonal variations of the 40-50 day oscillation in the tropics. *J. Atmos. Sci.*, 43, 3138-3158.

58. Madden, R. A., and P. Julian, 1971: Detection of a 40-50 day oscillation in the zonal wind. *J. Atmos. Sci.*, 28, 702-708.

59. Madden, R. A., and P. Julian, 1972: Description of global-scale circulation cells in the tropics with a 40-50 day period. *J. Atmos. Sci.*, 29, 1109-1123.

60. Madden, R. A., and P. Julian, 1994: Observations of the 40-50 day tropical oscillation – a review. *Mon. Wea. Rev.*,123, 814-837.

61. Madden, R. A., and P. Julian, 2005: Historical Perspective. *Intraseasonal Variability in the Atmosphere-Ocean Climate System*, K. M. Lau and D. E. Waliser, Eds., Praxis, 1-18.

62. Maloney, E. D., 2002: An intraseasonal oscillation composite life cycle in the NCAR CCM3.6 with modified convection. *J. Climate*, 15, 964-982.

63. Maloney, E. D., and D. L. Hartmann, 1998: Frictional moisture convergence in a composite life cycle of the Madden-Julian Oscillation. *J. Climate*, 11, 2387-2403.

64. Maloney, E. D., and D. L. Hartmann, 2000: Modulation of eastern North Pacific hurricanes by the Madden-Julian oscillation. *J. Climate*, 13, 1451-1460.

65. Maloney, E. D., and D. L. Hartmann, 2001: The sensitivity of intraseasonal variability in the NCAR CCM3 to changes in convective parameterization. *J. Climate*, 14, 2015-2034.

66. Maloney, E. D., and A. H. Sobel, 2004: Surface fluxes and ocean coupling in the tropical intraseasonal oscillation. *J. Climate*, 17, 4368-4386.

67. Maloney, E. D., and J. Shaman, 2008: Intraseasonal variability of the West African monsoon and the Atlantic ITCZ. *J. Climate*, 21, 2898-2918.

68. Maloney, E. D., 2009: The moist static energy budget of a composite tropical intraseasonal oscillation in a climate model. *J. Climate*, 22, 711-729.

69. Maloney, E. D., W. M. Hannah, and A. H. Sobel, 2009: Aquaplanet GCM simulations of intraseasonal moisture modes. In press.

70. Manabe, S., J. Smagorinsky and R. F. Strickler, 1965: Simulated climatology of a general circulation model with a hydrologic cycle. *Mon. Wea. Rev.,* 93, 769-798.

71. Mapes, B. E., 2000: Convective inhibition, subgrid-scale triggering energy, and stratiform instability in a toy tropical wave model. *J. Atmos. Sci.*, 57, 1515-1535.

72. Matthews, A. J., 2000: Propagation mechanisms for the Madden-Julian Oscillation. *Quart. J. Roy. Meteor. Soc*, 126, 2637-2651.

73. Matsuno, T., 1966: Quasi-geostrophic motions in the equatorial area. *J. Meteor. Soc. Japan*, 44, 25-43.

74. Mehta, A. V. and T. N. Krishnamurti, 1988: Interannual variability of the 30-50 day wave motions. *J. Meteor. Soc. Japan*, 46, 327-342.

75. Moorthi, S. and M. J. Suarez, 1992: Relaxed Arakawa-Schubert: A parameterization of moist convection for general circulation models. *Mon. Wea. Rev.,* 120, 978-1002.

76. Myers, D., and D. E. Waliser, 2003: Three-dimensional water vapor and cloud variations associated with the Madden-Julian oscillation during northern hemisphere winter. *J. Climate*, 16, 929-950.

77. Nakazawa, T., 1988: Tropical super clusters within intraseasonal variations over the western Pacific. *J. Meteor. Soc. Japan*, 66, 823-839.

78. Numaguti, A., M. Takahaski, T. Nakajima, and A. Sumi, 1995: Development of an atmospheric general circulation model. In *Reports of a New Program for Creative Basic Research Studies, Studies of Global Environment Change with Special Reference to Asia and Pacific Regions,* Rep. I-3, Center for Climate System Research, Tokyo, 1-27.

79. Neale, R. B., J. H. Richter, and M. Jochom, 2008: The impact of convection on ENSO: From a delayed oscillator to a series of events. *J. Climate*, 21, 5904-5924.

80. Neelin, J. D., I. M. Held, and K. H. Cook, 1987: Evaporation-wind feedback and low-frequency variability in the tropical atmosphere. *J. Atmos. Sci.* 44, 2341-2348.

81. Neelin, J. D., and I. M. Held, 1987: Modeling tropical convergence based on the moist static energy budget. *Mon. Wea. Rev.*, 115, 3-12.

82. Neelin, J. D., and J.-Y. Yu, 1994:Modes of tropical variability under convective adjustment and the Madden-Julian Oscillation. Part I: Analytical theory. *J. Atmos. Sci.*, 51, 1876-1894.

83. Park, C. K., D. M. Straus, and K.-M. Lau, 1990: An evaluation of the structure of tropical intraseasonal oscillations in 3 general circulation models. *J. Meteor. Soc. Japan*, 68, 403-417.

84. Peters, M. E., and C. S. Bretherton, 2006: Structure of tropical variability from a vertical mode perspective. *Theor. Comput. Fluid Dyn.*, doi:10.1007/s00162-006-0034-x.

85. Peters, O., and J. D. Neelin, 2006: Critical phenomena in atmospheric precipitation. *Nature Physics*, 2, 393-396,doi:10.1038/nphys314.

86. Raymond, D. J., 2001: A new model for the Madden-Julian Oscillation. *J. Atmos. Sci.*, 58, 2807-2819.

87. Raymond, D. J., and X. Zeng, 2005: Modelling tropical atmospheric convection in the context of the weak temperature gradient approximation. *Quart. J. Roy. Meteor. Soc.*, 131, 1301-1320.

88. Raymond, D. J., S. L. Sessions, and Z. Fuchs, 2007: A theory for the spinup of tropical depressions. *Quart. J. Roy. Meteor. Soc.*, 133, 1743-1754.

89. Raymond, D. J., and Z. Fuchs, 2009: Moisture modes and the Madden-Julian Oscillation. *J. Climate*, 22, 3031-3046.

90. Raymond, D. J., S. L. Sessions, A. H. Sobel, and Z. Fuchs, 2009: The mechanics of gross moist stability. *J. Adv. Mod. Earth Sys.*,1, Art. #9.

91. Salby, M. L., and H. H. Hendon, 1994: Intraseasonal behavior of clouds, temperature and motion in the tropics, *J. Atmos. Sci.*, 51, 2207-2224.

92. Simpson, J., 1971: On cumulus entrainment and one-dimensional models. *J. Atmos. Sci.,* 28, 449-455.

93. Simmons, A. J., S. Uppala, D. P. Dee, and S. Kobayashi, 2007: ERA-interim: New ECMWF reanalysis products from 1989 onwards. *ECMWF newsletter*, 110, 25-35.

94. Slingo, J. M and coauthors, 1996: Intraseasonal oscillations in 15 atmospheric general circulation models: Results from an AMIP diagnostic subproject. *Climate Dyn.*, 12, 325-357.

95. Sobel, A. H., J. Nilsson, and L. M. Polvani, 2001: The weak temperature gradient approximation and balanced tropical moisture waves. *J. Atmos. Sci.*, 58, 3650-3665.

96. Sobel, A. H., E. D. Maloney, G. Bellon, and D. Frierson, 2009: Surface fluxes and tropical intraseasonal variability: A reassessment. *J. Adv. Mod. Earth Sys.*, in press.

97. Sperber, K. R., J. M. Slingo, P.M. Inness, and W. K.-M. Lau, 1997: On the maintenance and initiation of the intraseasonal oscillations in NCEP/NCAR reanalysis and the GLA and UKMO AMIP simulations. *Climate Dyn.*, 13, 769-795.

98. Sperber, K. R., 2003: Propagation and vertical structure of the Madden-Julian Oscillation. *Mon. Wea. Rev.*, 131, 3018-3037.

99. Sperber, K. R., S. Gualdi, S. Legutke, V. Gaylor, 2005: The Madden-Julian Oscialltionin ECHAM4 coupled and uncoupled GCMs. *Climate Dyn.*, 25, 117-140.

100. Straub, K. H., and G. N. Kiladis, 2003: The observed structure of convectively coupled Kelvin waves: comparison with simple models of coupled wave instability. *J. Atmos. Sci.*, 60, 1655-1668.

101. Sud, Y. C., and A. Molod, 1988: The roles of dry convection, cloud-radiation feedback processes, and the influence of recent improvements in the

parameterization of convection in the GLA GCM. *Mon. Wea. Rev.*, 116, 2366-2387.

102. Sud, Y. C., and G. K. Walker, 1993: Microphyics of clouds with the relaxed Arakawa-Schubert scheme (McRAS). Part I: Design and evaluation with GATE phase III data. *J. Atmos. Sci.*, 56, 3196-3220.

103. Sugiyama, M., 2009a: The moisture mode in the quasi-equilibrium tropical circulation model. Part I: Analysis based on the weak temperature gradient approximation. *J. Atmos. Sci.*, 66, 1507-1523.

104. Sugiyama, M., 2009b: The moisture mode in the quasi-equilibrium tropical circulation model. Part II: Nonlinear behavior on an equatorial β plane. *J. Atmos. Sci.*, 66, 1525-1542.

105. Sui, C.-H. and K.-M. Lau, 1989: Origin of low-frequency (intraseasonal) oscillations in the tropical atmosphere. Part 2: Structure and propagation of mobile wave-CISK modes and their modification by lower boundary forcings. *J. Atmos. Sci.*, 46, 37-56.

106. Takahashi, M., 1987: Theory of the slow phase speed of the intraseasonal oscillation using the wave-CISK. *J. Meteor. Soc. Japan*, 65, 43-49.

107. Takayabu, Y. N., T. Iguchi, M. Kachi, A. Shibata, and H. Kanzawa, 1999: Abrupt termination of the 1997-98 El Niño in response to a Madden-Julian Oscillation. *Nature*, 402, 279-282.

108. Thayer-Calder, K. and D. A. Randall, 2009: The role of convective moistening in the formation and progression of the MJO. Submitted to *J. Atmos. Sci.*

109. Tian, B., D. E. Waliser, E. J. Fetzer, B. H. Lambrigsten, Y. Yung, and B. Wang, 2006: Vertical moist thermodynamic structure and spatial-temporal evolution of the MJO in AIRS observations. *J. Atmos. Sci.*, 63, 2462-2485.

110. Tokioka, T., K. Yamazaki, A. Kitoh and T. Ose, 1988: The equatorial 30-60 day oscillation and the Arakawa-Schubert penetrative cumulus parameterization. *J. Meteor. Soc. Japan,* 66, 883-901.

111. Uppala, S. M., and Coauthors, 2005: The ERA-40 reanalysis. *Quart. J. Roy. Meteor. Soc.*, 131, 2961-3012, doi:10.1256/qj.04.176.

112. Waliser, D. E., K. M. Lau, and J.-H. Kim, 1999: The influence of coupled sea surface temperatures on the Madden-Julian Oscillation: A model perturbation experiment. *J. Atmos. Sci.*, 56, 333-358.

113. Wang, B., 2005: Theories. *Intraseasonal Variability in the Atmosphere-Ocean Climate System*, K. M. Lau and D. E. Waliser, Eds., Praxis, 307-360.

114. Wang, B., 1988: Dynamics of tropical low-frequency waves: An analysis of the moist Kelvin wave. *J. Atmos. Sci.*, 45, 2051-2065.

115. Wang, B., and T. Li, 1994: Convective interaction with boundary-layer dynamics in the development of a tropical intraseasonal system. *J. Atmos. Sci.*, 51, 1386-1400.

116. Wang, B., and H. Rui, 1990: Dynamics of the coupled moist Kelvin-Rossby wave on an equatorial beta plane. *J. Atmos. Sci.*, 47, 397-413.

117. Wang, W., and M. E. Schlesinger, 1999: The dependence on convection parameterization of the tropical intraseasonal oscillation simulated by the UIUC 11-layer atmospheric GCM. *J. Climate,* 12, 1423-1457.

118. Wentz, F. J., and R. W. Spencer, 1998: SSM/I rain retrievals within a unified all-weather ocean algorithm. *J. Atmos. Sci.*, 55, 1613-1627.

119. Wheeler, M. C., and H. H. Hendon, 2004: An all-season real-time multivariate MJO index: Development of an index for monitoring and prediction. *Mon. Wea. Rev.*, 132, 1917-1932.

120. Wheeler, M. C., and G. N. Kiladis, 1999: Convectively coupled Equatorial waves: Analysis of clouds and temperature in the wavenumber-frequency domain. *J. Atmos. Sci.*, 56, 374-399.

121. Wu, M. L. C., S. Scubert, I. S. Kang, and D. E. Waliser, 2002: Forced and free intraseasonal variability over the South Asian monsoon region simulated by 10 AGCMs. *J. Climate*, 15, 2862-2880.

122. Xie, S.-P., A. Kubokawa, and K. Hanawa, 1993: Evaporation-wind feedback and the organizing of tropical convection on the planetary scale. Part II: Non-linear evolution. *J. Atmos. Sci.*, 50, 3884-3893.

123. Xie, S.-P., and P. A. Arkin, 1997: Global precipitation: A 17-year monthly analysis based on gauge observations, satellite estimates, and numerical model outputs. *Bulletin of the American Met. Soc.*, 78, 2539-2558.

124. Yasunari, T., 1979: Cloudiness fluctuations associated with the Northern Hemisphere summer monsoon. *J. Meteor. Soc. Japan*, 57, 227-242.

125. Yasunari, T., 1980: A quasi-stationary appearance of 30-40 day period in the cloudiness fluctuations during the summer monsoon over India. *J. Meteor. Soc. Japan*, 58, 225-229.

126. Yu, J.Y., C. Chou, and J. D. Neelin, 1998: Estimating the gross moist stability of the tropical atmosphere. *J. Atmos. Sci.*, 55, 1354-1372.

127. Yu, J.-Y., and J. D. Neelin, 1997: Analytic approximations for moist convectively adjusted regions. *J. Atmos. Sci.*, 54, 1054-1063.

128. Zhang, C., and M. Dong, 2004: Seasonality of the Madden Julian Oscillation, *J. Climate*, 17, 3169-3180.

129. Zhang, C., 2005: The Madden-Julian Oscillation. *Rev. Geophys.*, 43, RG2003, doi:10.1029/2004RG000158.

130. Zhang, C., M. Dong, S. Gualdi, H. H. Hendon, E. D. Maloney, A. Marshall, K. R. Sperber, and W. Wang, 2006: Simulations of the Madden-Julian Oscillation in four pairs of coupled and uncoupled models. *Climate Dyn.*, 27, 573-592.

131. Zhang, G. J., and N. A. McFarlane, 1995: Sensitivity of climate simulations to the parameterization of cumulus convection in the Canadian Climate Centre general circulation model. *ATMOS-Ocean,* 33, 407-446.

132. Zhang, G. J., 2002: Convective quasi-equilibrium in midlatitude continental environment and its effect on convective parameterization. *J. Geophy. Res.,* 107, 4220, doi:10.1029/2001JD001005.

133. Zhang, G. J., and M. Mu, 2005: Simulation of the Madden-Julian Oscillation in the NCAR CCM3 using a revised Zhang-McFarlane convection parameterization scheme. *J. Climate,* 18, 4046-4064.

134. Zheng, Y., D. E. Waliser, and W. F. Stern, 2004: The role of coupled sea surface temperatures in the simulation of the tropical intraseasonal oscillation. *J. Climate*, 17, 4109-4134.